



Title	傾斜板上液膜流れの挙動
Author(s)	戸村, 芳
Citation	大阪大学, 1979, 博士論文
Version Type	VoR
URL	https://hdl.handle.net/11094/2733
rights	
Note	

The University of Osaka Institutional Knowledge Archive : OUKA

<https://ir.library.osaka-u.ac.jp/>

The University of Osaka

**BEHAVIOR
OF
FALLING LIQUID FILMS
ON
INCLINED PLATES**

Kaoru TOMURA

**Department of Chemical Engineering
Faculty of Engineering Science
Osaka University
1979**

CONTENTS

	page
Chapter 1	General Introduction ----- 1
Chapter 2	Velocity Profile in Calming Zone
	----- 9
	Introduction ----- 10
	1. Experimental Apparatus and Procedure ----- 12
	2. Observation of Film Surface -- 15
	3. Analysis ----- 20
	4. Results and Discussion ----- 22
	Conclusion ----- 28
Chapter 3	Thickness of Falling Liquid Film in Calming Zone ----- 32
	Introduction ----- 33
	1. Analysis ----- 34
	2. Results and Discussion ----- 39
	Conclusion ----- 44

CHAPTER 1

GENERAL INTRODUCTION

Falling liquid film flows are common in everyday life and have numerous applications in modern technology. The study on the film flow started at the beginning of the twentieth century and is still in active progress. Fulford⁷⁾ summarized a number of investigations on liquid thin films published before 1964. In this chapter, the subsequent (from 1965 up to the present) investigations will be reviewed briefly.

On the subject of film thickness, the measurements have been correlated with Re separately in wavy and in turbulent regions. Even in the same region, there are as many correlation curves^{4,13,18,20)} as the number of investigators, and they deviate each other significantly and sometimes systematically. However, no adequate explana-

tions to the deviations have been presented yet.

In the literature, no clear descriptions on the positions of measurements and on the liquid inlet conditions were made, because fully developed flows were assumed. However, it is considered that the measurement positions and inlet conditions could cause systematic deviations of the correlations. In this work, the measurements have been carried out with special attention to these problems.

The surface behavior of falling liquid films can be classified into two patterns, that is, undisturbed mirror-like zone and regularly or irregularly disturbed zone, by which film flows are characterized. Initially, a smooth region can be observed before the wave inception on the film surface. A number of critical flow conditions were proposed, but none of them took into account the positions from the inlet.

The interrelation between "entry" and "accelerating zone (with core flow)" was not made clear, and there were no systematic and quantitative studies on "smooth zone". Therefore, this relation and the longitudinal film thickness variation will be discussed in Chapter 3.

According to the studies on stability^{5,7,19,21,30)} for the various flow conditions, the film flows are almost always unstable unless Re is very low. However, the positions from the inlet have not been taken into account at all.

In Chapter 4, the position of wave inception will be studied to give an adequate explanation for the mechanism of the smooth zone.

As the flow rate increases, the film surface comes to be covered partially with waves. The character of waves on film surfaces has been investigated experimentally^{11,25,36)} and theoretically^{2,3,16,26,27,34)}, but the results are not successful. It is well known that the waves on films are not periodic but vary irregularly with time⁷⁾, and it was described²⁵⁾ that the characters of waves depended very much on the positions. This may be the cause of difficulty in theoretical treatments and of a scatter of experimental data.

The importance of a knowledge on the velocity profiles within falling liquid films under various flow conditions was stressed by many investigators, and a few measurements for special cases were reported in spite of the difficulty caused by the film thickness. And many workers discussed the

ratio of surface velocity to average velocity that would be an indication of velocity profile, but the results have not been unified yet. In Chapter 2, the velocity profile in "calming zone" of film on inclined plate will be discussed.

To study the hydrodynamics of the falling liquid flows is essential to the predictions of mass transfer rates between a falling liquid film and the adjoining phase. The rates seemed to be influenced by the surface behavior¹²⁾. It is described in Chapter 4 that the position of wave inception affects the mass transfer rate significantly. The relation between instantaneous local mass transfer rates³⁹⁾ and the simultaneous film thickness in "rippling zone" will be discussed in Chapter 5.

The increase of interfacial area in a wavy film leads to the increase of the mass transfer rate between the film and the adjacent gas phase. Recently, the new approaches^{24,28)} without "two-dimensional" assumption which was common in early days, have been reported and they show that the increase of interfacial area is small under ordinary flow conditions.

It is well known that surface-active materials

can damp many types of waves, and reduce the mass transfer rate at a given liquid flow rate. This effect is still under investigating theoretically (14,31,35,37) and experimentally^{33,36)}.

Film flows of non-Newtonian fluids become important increasingly, such as in polymer production, in biochemical and physiological processes, in waste disposal systems and so on. And recently, several experimental^{15,29)} and theoretical^{22,32)} studies have been reported. The problems of rupture of a thin liquid falling film (17,23), of droplet removal movement^{1,10,38)} and of the flow regime for concurrent flow³⁵⁾ have been investigated. However, these are main unresolved problems in these fields.

The purpose of this work is to investigate the longitudinal variation of the behavior of falling liquid films on inclined plates.

Literature Cited

- 1) Anderson, R.J. and T.W.F. Russell: AIChE J., 16, 626(1970)
- 2) Byatt-Smith, J.G.B.: *ibid.*, 17, 557(1971)
- 3) Byatt-Smith, J.G.B.: J. Fluid Mech., 49, 625(1971)
- 4) Collier, J.G. and G.F. Hewitt: Brit. Chem. Eng., 12, 709(1967)
- 5) Demekhin, E.A.: Fluid Dynamics, 10, 126(1976)
- 6) Freeman, N.C.: J. Fluid Mech., 56, 257(1972)
- 7) Fulford, G.D.: "Advanced in Chemical Engineering" 5, 151, Academic Press(1964)
- 8) Hartland, S.: Chem. Eng. Sci., 26, 257(1971)
- 9) Holmes, D.B. and J.R. Vermeulen: *ibid.*, 23, 717(1968)
- 10) Hughmark, G.A.: AIChE J., 19, 1062(1973)
- 11) Javdani, K.: *ibid.*, 22, 867(1976)
- 12) Kawai, M.: Master Thesis (Osaka Univ.) (1971)
- 13) Koski, P.G.: Int. J. Heat Mass Transfer, 14, 1220(1971)
- 14) Lin, S.P.: AIChE J., 16, 375(1970)
- 15) Mashelkar, R.A. and M.A. Soylu: Chem. Eng. Sci., 29, 1089(1974)
- 16) Massot, C., F. Irani and E.N. Lightfoot: AIChE J., 12, 445(1966)

- 17) Mikielwicz, J. and J.R. Moszynski:
Int. J. Heat Mass Transfer, 19,771 (1976)
- 18) Murthy, V. N. and P.K. Sarna: Chem. Eng. Sci.,
29,1659 (1974)
- 19) Nakaya, C. and R. Takaki: J. Phys. Soc. Japan,
23,638 (1967)
- 20) Nakajima, T.,: Master Thesis (Osaka Univ.)(1972)
- 21) Nepomngyashchii,A.A.: Fluid Dynamics,9,351(1975)
- 22) Pendergrass, J.: AIChE J.,21,487 (1975)
- 23) Ponter, A. B. and K. M. Aswald: Int. J. Heat
Mass Transfer,20,575 (1977)
- 24) Portalski, S. and A.J. Clegg: Chem. Eng. Sci.,
26,773 (1971)
- 25) Portalski, S.: AIChE J.,19,1244 (1973)
- 26) Roskes, G. J.: Phys. Fluids.,13,1440 (1970)
- 27) Rushton, E. and G.A. Davies: AIChE J.,17,
670 (1971)
- 28) Shilimkan, R. V. and J.B. Stepanek: Chem. Eng.
Sci.,32,149 (1977)
- 29) Skelland, A. H. P. and V. O. Popadic: AIChE J.,
21,861 (1975)
- 30) Smith, F. I. P.: Phys. Fluids,13,1693 (1970)
- 31) Smith, F. I. P. and A. D. D. Craik: J. Fluid
Mech.,45,527 (1971)
- 32) Srivastava, R. P. S.: Chem. Eng. Sci.,28,819(1973)

- 33) Storobel, W. J. and S. Whitaker: AICHE J., 15,
527 (1969)
- 34) Takaki, R.: J. Phys. Soc. Japan, 27, 1648 (1969)
- 35) Taitel, Y, and A. E. Dukler: AICHE J., 22
47 (1976)
- 36) Tsuboi, N.,: Master Thesis (Osaka Univ.) (1973)
- 37) Whitaker, S. and L.O. Jones: AICHE J., 12, 421 (1966)
- 38) Woodmansee, D. E. and T. J. Hanratty: Chem. Eng.
Sci., 24, 299 (1969)
- 39) Yamamoto, M.: Master Thesis (Osaka Univ.) (1974)

CHAPTER 2

VELOCITY PROFILE

IN CALMING ZONE

Abstract

Falling liquid films on inclined plates have been experimentally studied in the range of Re from 2500 to 6000, with special attention to the "calming zone" where the surface is mirror-like.

Velocity profile by the hydrogen bubble method and film thickness by the pointer and gauge method were measured, and film surface behavior has been observed by laser beam reflection.

Film flow in the calming zone is laminar with air drag at the liquid interface.

Introduction

Flow of falling liquid film is frequently observed in chemical plants. Typical applications of film flow in process are in packed towers and various types of coolers and evaporators.

A knowledge of the velocity profiles within falling films under various flow conditions is important, making it possible to calculate the rates of convective heat and mass transfer processes.

The thinness of most liquid films makes it difficult to measure the velocity profiles. A few techniques have been proposed for the measurement of the velocity profile in thin film, and classified as :

- (i) Stereoscopic photography method^{7,15)},
- (ii) "Hot-wire" method¹⁾,
- (iii) Photographic tracer method^{4,5)} and
- (iv) Hydrogen bubble visualization method¹³⁾.

For $Re < 2500$, the velocity distribution measured by these methods agreed with the classical analysis by Nusselt in which two-dimensional fully developed laminar flow and no

drag at the air-liquid interface were assumed.

The flow was laminar without rippling for $Re < 24$, and became pseudo-laminar with rippling and then turbulent with increasing Reynolds number^{4, 15}).

The state of falling liquid film ($Re > 24$) has been classified into several zones according to the behavior of liquid surface as follows :

"rippling zone" where periodic waves are present at the surface,

"calming zone" where the surface is wave-free and mirror-like, and

"turbulent zone" where the surface is randomly disturbed. These zones depend not only on

Reynolds number but also on the distance from the entrance.

When the films were falling onto vertical plates, the area of calming zone was small^{3,8,11, 12}).

However, on inclined plates, little is known about this zone. At a fixed point, calming zone is observed at higher Reynolds number than is rippling zone. It is interesting to know if the flow in calming zone is laminar or not.

To make this problem clear, the behavior of film surface has been observed using laser beam reflection. The velocity distribution in

calming zone has been measured by the hydrogen bubble method and is analyzed by taking account of the drag at air-liquid surface. Also, the film thickness has been measured directly by the pointer and gauge method, and this is compared with the analytical result.

1. Experimental Apparatus and Procedure

Deionized water was used as liquid and circulated by a pump. The inclined flat smooth plate, made of acrylic resins, is 16.5cm wide and 160cm long.

To measure the film thickness, a pointer and a gauge were set at 80cm ($x/h \sim 500$) from the entrance under the conditions of plate inclination of 6.2° , 8.9° and 14.8° to the horizon. To observe the behavior of the film surface, a laser beam was reflected to a certain direction in response to the shape of air-liquid surface and the images projected on the screen were photographed as shown in Fig. 3.

25 μ m-dia. polished tungsten wire was used as the cathode for the production of hydrogen bubbles. Through the plate, rows of hydrogen bubbles can be observed. An electrical pulse generator, a frequency counter, a stroboscope controlled by the pulse generator, and a camera were used for the measurements of velocity profiles in films. The wire was oriented diagonally through the film perpendicular to the main flow direction. A small amount of NaHCO₃ was added to adjust the electrical conductivity. The inclination angles of the flat plate were 7.4°, 8.9° and 17.2°. The velocity profiles were measured at 67cm (x/h~500) and 115cm (x/h~900) from the entrance, and the experimental range of Reynolds number was from 2500 to 6000. Figure 1 shows a typical example of hydrogen bubble rows.

There are some limitations in application of the hydrogen bubble method to velocity measurements in thin films. The velocity near the liquid surface is very high (more than 100 cm/sec). On the other hand, very close to the wall, the velocity is low as compared to the rising velocity of a fine bubble by buoyancy, and the velocity gradient is so large that the local velocities

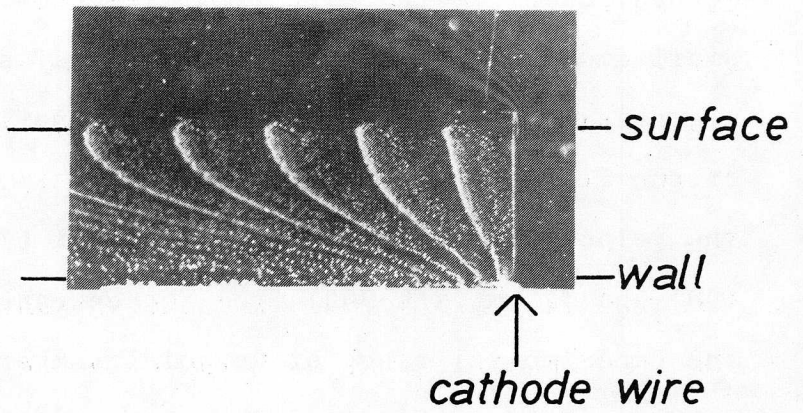


Fig. 1 Typical bubble rows $\theta=7.4^\circ$,
 $\theta=7.4^\circ$, $Re=4900$,
pulse interval=5.40ms

cannot be measured accurately. Thus the velocity observed near the wall has a tendency to be higher than the real one. The data near the wall of Thomas and Rice¹³⁾ by the hydrogen bubble method showed a systematic deviation from their correlation curve. The author has disregarded the data near the wall ($y/h \leq 0.2$). Because the wire and liquid surface may cause a capillary effect, the first and second rows of hydrogen bubbles behind the wire have also been disregarded. The Reynolds numbers based on the maximum liquid velocity and on the tungsten wire diameter were kept below 40 to prevent vortex shedding and to maintain sharp rows of bubbles¹³⁾.

The conditions of two-dimensional flow required for the hydrogen bubble method are given by Hopf's theoretical analysis⁶⁾. The assumption of fully developed flow is numerically confirmed by the reports of Bruley²⁾ and of Stüchel and Özisik¹⁰⁾.

2. Observation of Film Surface

Typical examples of photographs of three different zones of film surfaces are shown in Fig. 2. Rippling zone is characterized by the existence of regular rows of waves. This regularity makes the laser beam reflected onto the screen walk one-dimensionally like the motion of a piston (Fig. 3a). On the other hand, in the turbulent zone the reflected laser beam walks two-dimensionally, at random and quickly due to the surface irregularly disturbed (Fig. 3c). Calming zone is characterized by the smooth surface, and the beam continues to stand at one point on the screen (Fig. 3b).

Figure 4 shows the variation of film thickness at a fixed point ($x/h=500$) against Reynolds number. It can be seen that the transition to turbulent from calming occurs at $Re \sim 10000$, and that from rippling to calming at $Re \sim 2500$, that is, calming zone appears at higher Re than does rippling zone. However, it was reported in the literature^{4,11,15}) that $Re \sim 2000$ was the transition from rippling to turbulent and calming zone was not recognized. It is observed in this study that the length of calming zone has a maximum at Reynolds number about 6000, that is, as the flow rate

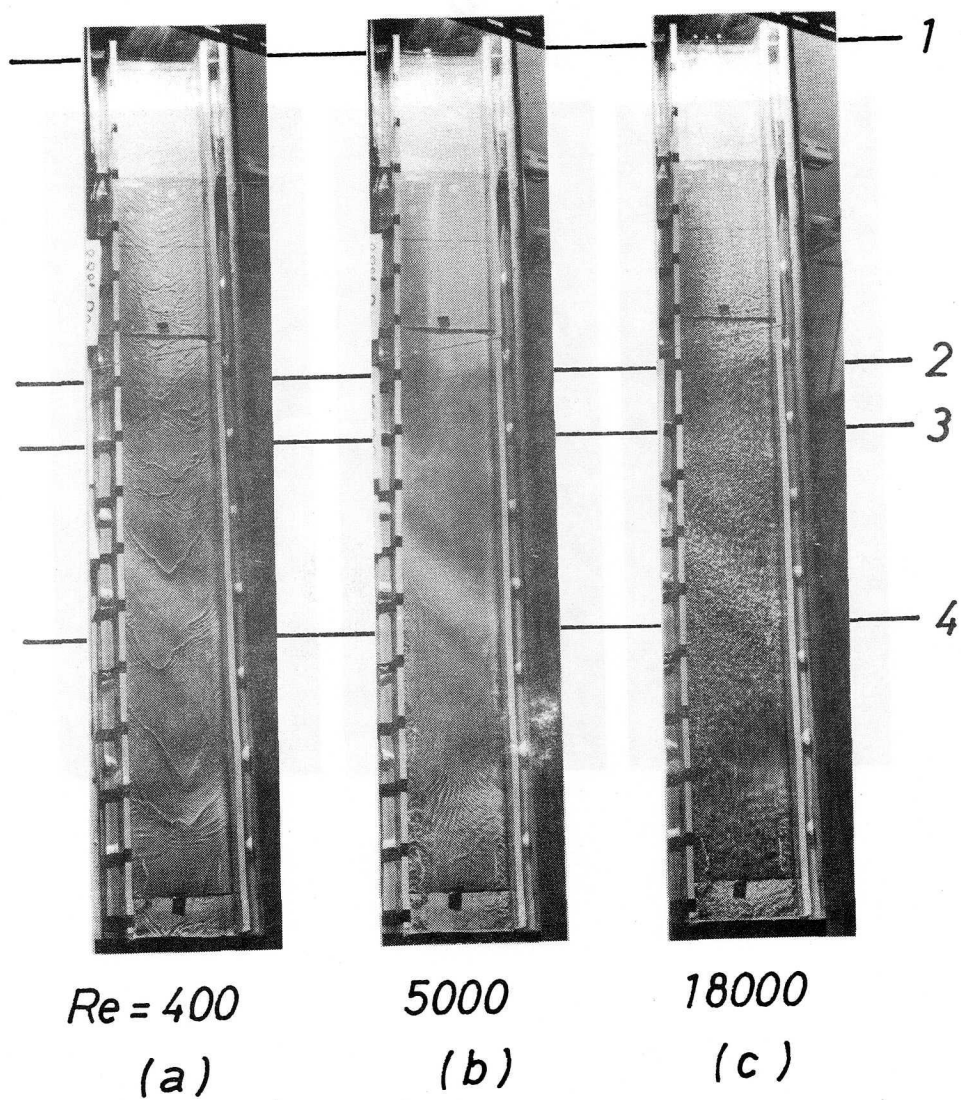


Fig. 2 Film surfaces

$\theta = 8.9^\circ$, (a) $Re = 400$ (b) $Re = 5000$ (c) $Re = 18000$

Positions ; 1=the entrance, 2 and 4=for velocity profile measurements, 3=for film thickness measurements

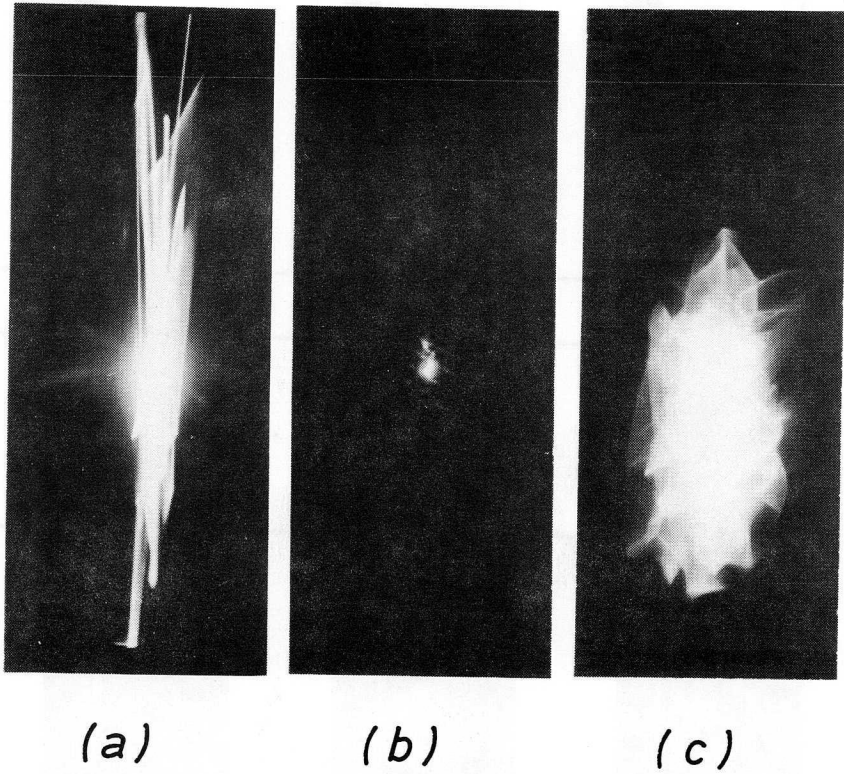


Fig. 3 Projected images of laser beam reflection
(a) Rippling zone (b) Calming zone
(c) Turbulent zone
(Scales in each photo. are the same.)

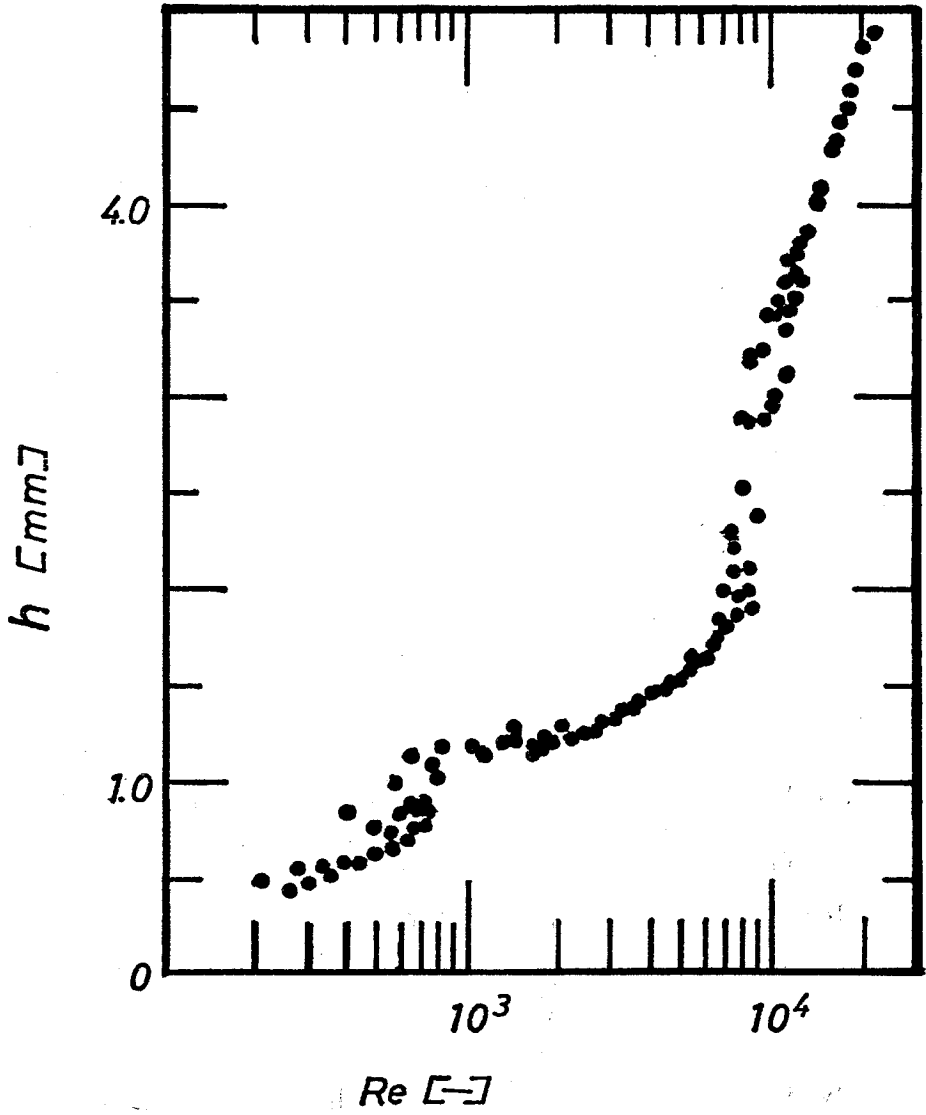


Fig. 4 Variation of film thickness at a fixed point, ($\theta=8.9^\circ$) ($x=80\text{cm}$)

increases, calming zone increases and then decreases. The relation between the length of calming zone and flow rate will be discussed in Chapter 4.

3. Analysis

The equation of motion for fully developed and laminar flow should be solved with two boundary conditions, that is, no slip condition at wall and the continuity of shear stress at air-liquid interface. However, the following velocity profile is assumed in this work, because the analytical or numerical solutions are troublesome to treat. Therefore, u_{s*} and h_* in Eq.(1) are determined experimentally.

$$u_* = u_{s*} \eta + \frac{1}{2} h_*^2 \eta (1-\eta) \quad (1)$$

By integrating Eq.(1) over the film thickness, one obtains

$$Re = \frac{1}{3} h_*^3 + 2h_* u_{s*} \quad (2)$$

Shear stresses at the surface and at the wall are given by Eqs.(3) and (4), respectively.

$$\tau_{S*} = \frac{u_{S*}}{h_*} - \frac{1}{2}h_* \quad (3)$$

$$\tau_{W*} = h_* + \tau_{S*} \quad (4)$$

From Eq.(1), u/η should be a linear function of η .

It is convenient to introduce the parameter K , defined by Eq.(5), which indicates the shift from Nusselt's analysis (no drag at the air-liquid surface) :

$$u_{S*} = \frac{1}{2}(1-K)h_*^2 \quad (5)$$

From Eqs.(2), (3), (4) and (5), the following equations are derived.

$$h_* = Re^{1/3} / \left(\frac{4}{3} - K\right)^{1/3} \quad (6)$$

$$u_{S*} = \frac{1}{2}(1-K)Re^{2/3} / \left(\frac{4}{3} - K\right)^{2/3} \quad (7)$$

$$\tau_{S*} = -\frac{1}{2}K \cdot Re^{1/3} / \left(\frac{4}{3} - K\right)^{1/3} \quad (8)$$

$$u_* = \left\{ \left(1 - \frac{1}{2}K\right)\eta - \frac{1}{2}\eta^2 \right\} Re^{2/3} / \left(\frac{4}{3} - K\right)^{2/3} \quad (9)$$

For $K=0$, these equations are reduced to Nusselt's equations as follows :

$$h^+ = \sqrt{3Re}/2 \quad (10)$$

$$u_s^+ = \sqrt{3\text{Re}}/4 \quad (11)$$

$$\tau_s = 0 \quad (12)$$

$$u^+ = y^+ - y^{+2}/\sqrt{3\text{Re}} \quad (13)$$

4. Results and Discussion

Velocity measurements have been carried out in the calming zone. An example of $u/(y/h)$ vs. y/h is shown in Fig. 5. These are correlated well with a straight line and the variance on each run is less than 1.4%. And also no velocity fluctuation was observed in the preliminary test by the "hot-wire" method. It is proved that the flow in calming zone on inclined plates is laminar in spite of Reynolds numbers higher than 2000. This conclusion is similar to that of Ho and Hummel⁵⁾ who observed no turbulent motion even at a Reynolds number of 3000 within falling liquid films inside a vertical tube. By the method of least squares, to the correlation of u/η vs η , the values of h_* and u_{s*} are determined for each run,

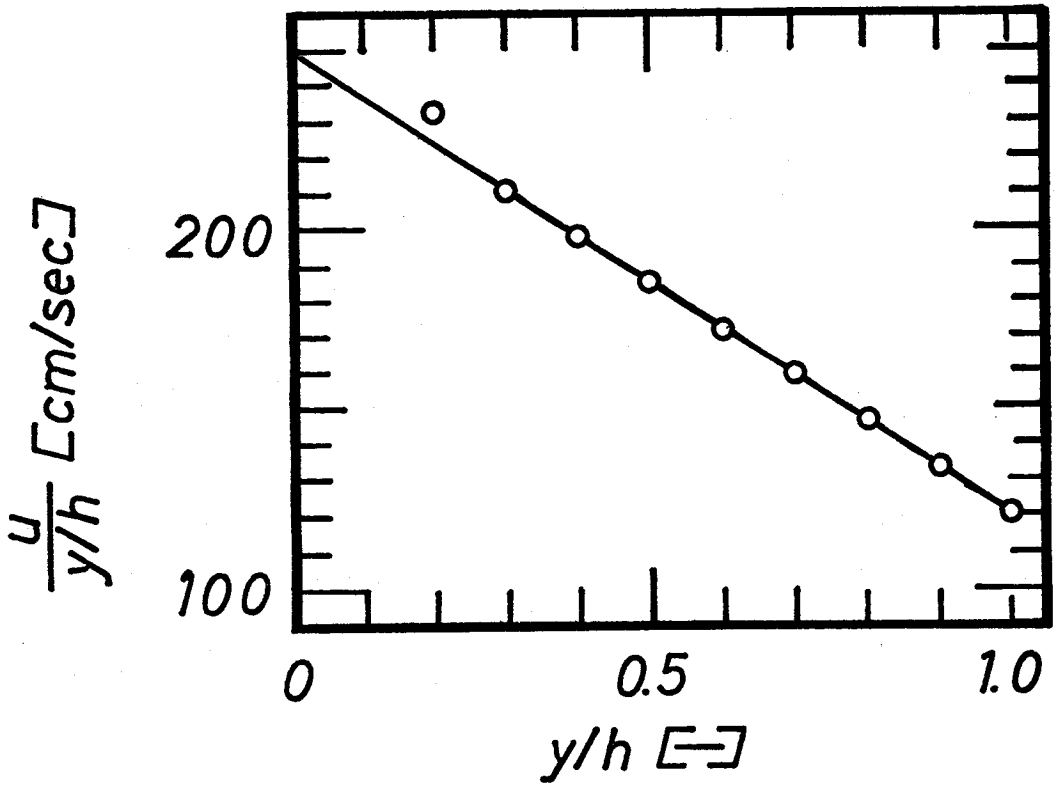


Fig. 5 Correlation of u/η vs η
 $Re=4900$, $\theta=7.4^\circ$, $x=67\text{cm}$

and shown on logarithmic scales in Fig. 6. The correlation gives the slope as 2 and the average value of K as follows ;

$$K = 0.134 \quad (14)$$

Substituting Eq.(14) into Eqs.(4), (6) and (8), one obtains $\tau_s/\tau_w = -0.0718$ regardless of Re, that is, τ_s is not negligible as compared to τ_w . The ratio of u_s to the average velocity is 1.39, and u_{s*} is smaller than Nusselt's analysis as shown in Fig. 7 with the result of West and Cole¹⁴).

The film thickness estimated from Eq.(6) is compared with direct measurements by the pointer and gauge method in Fig. 8 and good agreement is obtained. The volumetric flow rate estimated by Eq.(2) coincides with the measurement by a flow meter.

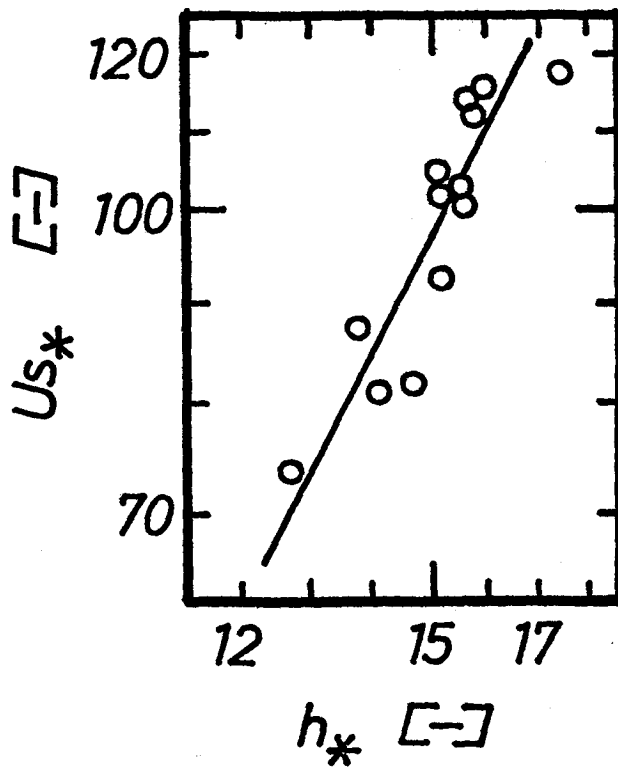


Fig. 6 Correlation of surface velocity with film thickness

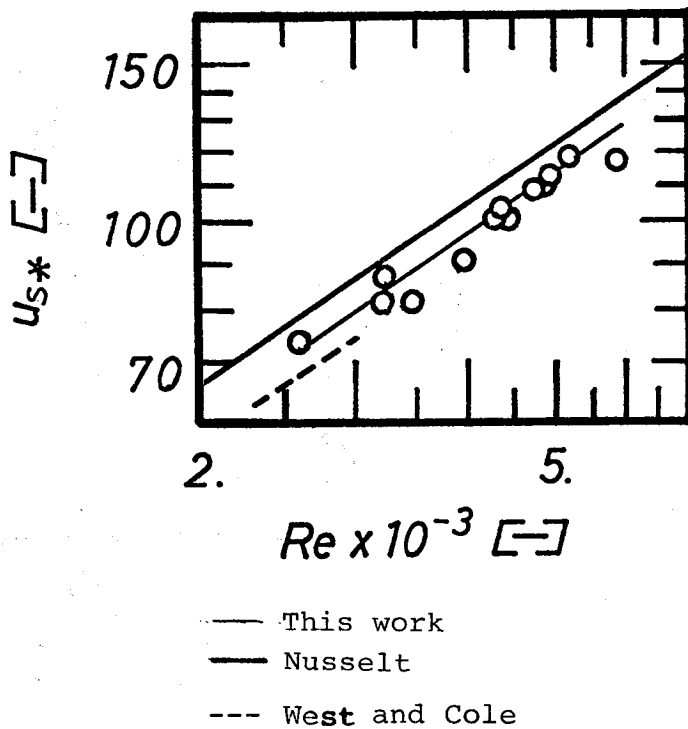


Fig. 7 Correlation of surface velocity with Reynolds number

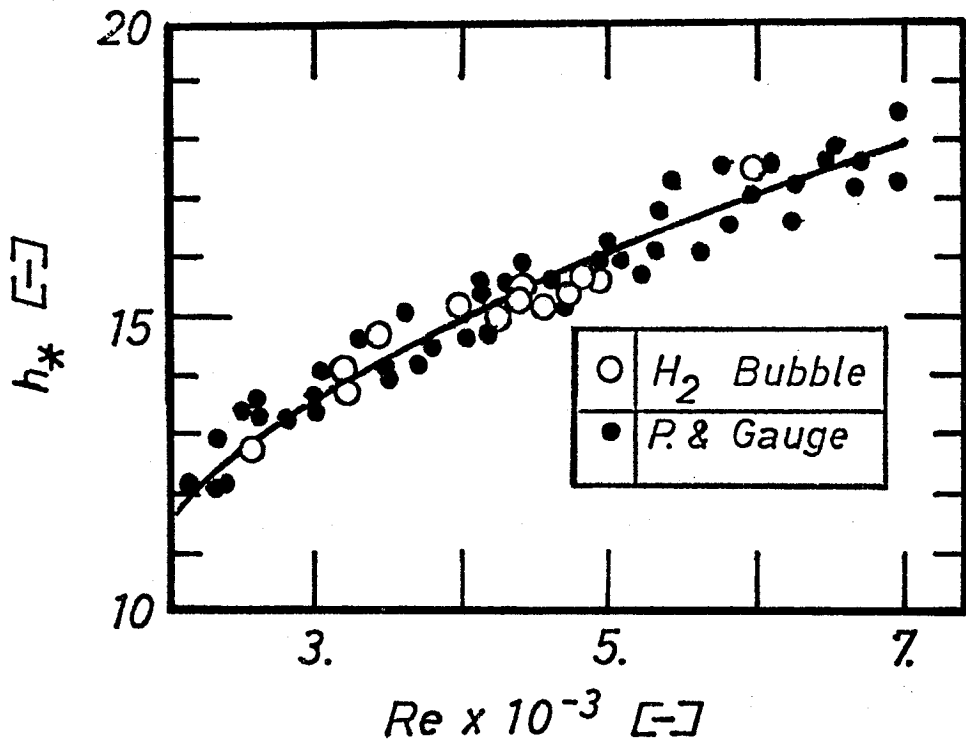


Fig. 8 Comparison of film thickness by pointer and gauge method and based on hydrogen bubble method

Conclusion

In falling liquid film on inclined plates, the flow behavior is classified into three zones ; rippling, calming and turbulent zones based on surface structure and variation of film thickness, the region of which depends on flow rate and distance from the entrance. The calming zone, characterized by the wave-free and mirror-like surface, is observed in the range of Re from 2000 to 6000 at a distance of $x/h \sim 500$. The flow in this zone is laminar in spite of Reynolds number higher than 2500. The velocity distribution has been measured by the hydrogen bubble method and expressed by Eq.(9) with Eq.(14), which have been derived by assuming two-dimensional, fully developed laminar flow with drag of air.

The shear stress at the air-liquid surface is not negligible but considerably affects the velocity distribution.

The direct measurements of film thickness coincide with the estimations based on the hydrogen bubble method.

Nomenclature

h	= liquid film thickness	[cm] or [mm]
h_*	= $h(g \sin\theta)^{1/3}/\nu^{2/3}$	[-]
h^+	= $h\sqrt{\tau_w/\rho}/\nu$	[-]
K	= parameter defined by Eq.(5)	[-]
Q	= $u \cdot h$	[cm ² /sec]
Re	= $4Q/\nu$	[-]
u	= fluid velocity	[cm/sec]
u_*	= $u/(\nu g \sin\theta)^{1/3}$	[-]
u^+	= $u_*/\sqrt{\tau_{w*}} = u/\sqrt{\tau_w/\rho}$	[-]
x	= distance from the entrance	[cm]
y	= coordinate axis	[cm]
y^+	= $y(g \sin\theta)^{1/3}\sqrt{\tau_{w*}}/\nu^{2/3} = y\sqrt{\tau_w/\rho}/\nu$	[-]
η	= y/h	[-]
θ	= inclination of plate to horizon	[deg]
ν	= kinematic viscosity of liquid	[cm ² /sec]
τ	= shear stress	[g/cm·sec ²]
τ_*	= $\tau/\rho(\nu g \sin\theta)^{2/3}$	[-]

<subscripts>

s	= at surface
w	= at wall

Literature Cited

- 1) Atkinson, B. and P.A. Caruthers: Trans. Instn. Chem. Engrs., 43, T33(1965)
- 2) Bruley, D.F.: AIChE J., 11, 945(1965)
- 3) Cerro, R.L. and S. Whitaker: Chem. Eng. Sci., 26, 742(1971)
- 4) Cook, R.A. and R.H. Clark: Can. J. Chem. Eng., 49, 412(1971)
- 5) Ho, F.C.K. and R.L. Hummel: Chem. Eng. Sci., 25, 1225(1970)
- 6) Hopf, L.: Ann. Physik, 32, 777(1910)
- 7) Nedderman, R.M.: Chem. Eng. Sci., 16, 113(1961)
- 8) Portalski, S. and A.J. Clegg: *ibid.*, 27, 1257(1972)
- 9) Portalski, S.: *ibid.*, 19, 575(1964)
- 10) Stüchel, A. and M.N. Özisik: *ibid.*, 31, 369(1976)
- 11) Tailby, S.R. and S. Portalski: *ibid.*, 17, 283(1962)
- 12) Tailby, S.R. and S. Portalski: Trans. Instn. Chem. Engrs., 40, 114(1962)
- 13) Thomas, W.C. and J.C. Rice: Trans. ASME Ser. E, 40, 321(1973)

- 14) West, D. and R. Cole: Chem. Eng. Sci., 22,
1388(1967)
- 15) Wilkes, J.O. and R.M. Nedderman: *ibid.*, 17,
177(1962).

CHAPTER 3

THICKNESS OF FALLING LIQUID FILM

IN CALMING ZONE

Abstract

The velocity profile described in Chapter 2 is applied to establish a simple flow model in calming zone. Based on the model, the longitudinal variations of film thickness are estimated and the values agree with the measurements at a fixed point. "Entrance length" calculated by the model agrees with that numerically solved by Bruley.

Introduction

Film thickness variation has been studied numerically^{1,2,6)} and analytically for falling liquid films on inclined plates^{2,7,8)} and vertical walls^{1,3,4)}. The drag of air at the liquid surface has been neglected in the previous work, but is not negligible, as is described in Chapter 2.

In this chapter, the variation will be discussed analytically by use of a flow model based on the velocity profile measurements.

Attention was given to "entrance length" in order to confirm that a flow at a position was fully developed or not. And the lengths for various types of film flows were estimated.

The terms "fully developed", "developed", "entrance" and "accelerating" zones were used confusedly in the previous work. Based on the flow model, "initial" and "developed" zones will be defined and in addition "entrance" zone will be conventionally introduced. The relation of the lengths of these zones will be discussed.

1. Analysis

Assuming the boundary layer approximations, and neglecting the pressure gradient, one can obtain Eq.(1) as a simplified form of equation of motion for incompressible fluid.

$$\begin{aligned}
 - \frac{d}{dx} \int_0^h u^2 dy + u_s \frac{d}{dx} \int_0^h u dy + g \sin \theta \cdot h \\
 = \nu \left\{ \left(\frac{\partial u}{\partial y} \right)_w - \left(\frac{\partial u}{\partial y} \right)_s \right\}
 \end{aligned} \tag{1}$$

and the continuity equation is

$$\int_0^h u dy = \frac{\nu}{4} Re \tag{2}$$

and Re is a constant for incompressible fluid at steady state. Equations (1) and (2) are transformed into dimensionless forms as follows, respectively.

$$\begin{aligned}
 - \frac{d}{dx_*} \int_0^{h_*} u_*^2 dy_* + u_{s*} \frac{d}{dx_*} \int_0^{h_*} u_* dy_* + h_* \\
 = \tau_{w*} - \tau_{s*}
 \end{aligned} \tag{3}$$

$$\int_0^{h_*} u_* dy_* = \frac{Re}{4} \tag{4}$$

Equations (5), (6) and (7) are parts of the experimental results under steady, fully developed flow

conditions, as given in Chapter 2.

$$u_*(\eta) = \eta(u_{s*} + \frac{1}{2}h_*^2) - \frac{1}{2}h_*^2\eta^2 \quad (5)$$

$$-\tau_{s*} = \frac{K}{2(1 - \frac{1}{2}K)} \tau_{w*} \quad (K=0.134) \quad (6)$$

$$h_* = Re^{1/3} / (\frac{4}{3} - K)^{1/3} \quad (7)$$

The velocity profile, Eq.(5), is modified to get the flow model as shown in Fig. 1. Based on the velocity profile, the "initial" and "developed" regions are defined as follows :

Initial region ($0 \leq x_* \leq x_{1*}$) where a core region exists, is followed by developed region ($x_{1*} \leq x_*$) where a core disappears and normalized velocity profile is similar but film thickness decreases downstream. In initial region the boundary layer thickness $\delta_*(x_*)$ increases and the core depth $c_*(x_*)$ decreases with increasing x_* , and at $x_* = x_{1*}$, c_* becomes zero (see Fig. 1).

For the initial region

$$u_*(x_*, y_*) = u_{c*} \left\{ 2 \left(\frac{y_*}{\delta_*} \right) - \left(\frac{y_*}{\delta_*} \right)^2 \right\}, \text{ for } 0 \leq y_* \leq \delta_* \quad (8)$$

$$u_* = u_{c*}, \quad \delta_* \leq y_* \leq \delta_* + c_* \quad (9)$$

$$u_* = u_{c_*} \left\{ 2 \left(\frac{y_* - c_*}{\delta_*} \right) - \left(\frac{y_* - c_*}{\delta_*} \right)^2 \right\}, \text{ for } \delta_* + c_* \leq y_* \leq h_* \quad (10)$$

where $u_{c_*}(x_*)$ is derived from Bernoulli's equation as follows :

$$u_{c_*}^2 = u_{o_*}^2 + 2x_* \quad (11)$$

For the developed region,

$$u_*(x_*, y_*) = u_{c_*} \left\{ 2 \left(\frac{y_*}{\delta_*} \right) - \left(\frac{y_*}{\delta_*} \right)^2 \right\}, 0 \leq y_* \leq h_* \quad (12)$$

Assuming that the ratio τ_{s_*}/τ_{w_*} at any position x is constant $(1-\alpha)$, Eq.(13) is written.

$$\tau_{w_*}(x_*) - \tau_{s_*}(x_*) = \alpha \tau_{w_*}(x_*) \quad (13)$$

α is given by Eq.(14) for initial region and Eq.(15) for developed region.

$$\alpha = (h_* - c_*)/\delta_* \quad (14)$$

$$\alpha = h_* / \delta_*' \quad (15)$$

Putting these velocity profiles into Eq.(4), one obtains Eqs.(16) and (17) for initial region and developed region, respectively.

$$c_* = \frac{Re}{4u_{c_*}} - \alpha^2 \left(1 - \frac{\alpha}{3} \right) \cdot \delta_* \quad (16)$$

$$u_{c_*} = \frac{Re}{4\alpha \left(1 - \frac{1}{3}\alpha \right) \cdot h_*} \quad (17)$$

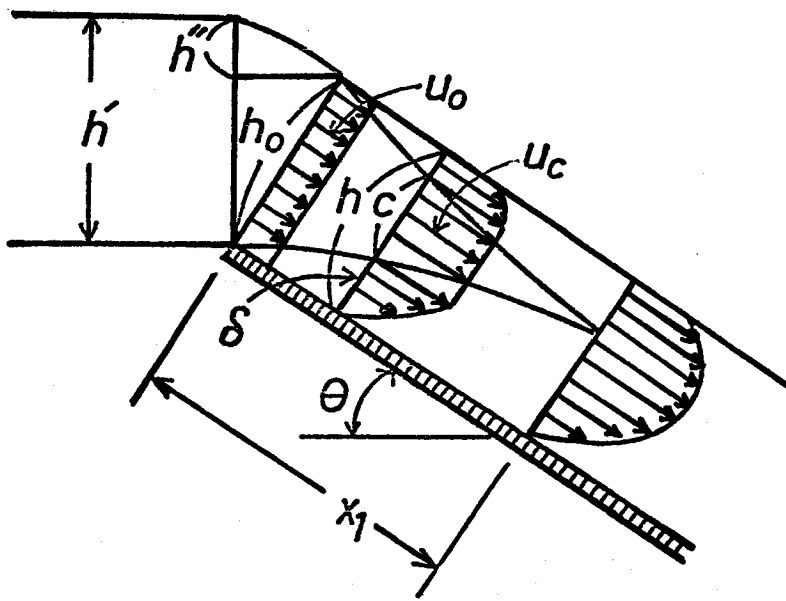


Fig. 1 Schematic of flow model considered

With the initial condition $\delta_* = 0$ at $x_* = 0$, Eqs.(18), (19) and (20) are derived for the initial region ($0 \leq x_* \leq x_{1*}$).

$$h_* = \frac{Re}{4u_{c*}} + \alpha \left\{ 1 - \alpha \left(1 - \frac{1}{3}\alpha \right) \right\} \delta_* \quad (18)$$

$$\delta_* = \sqrt{3} (u_{c*} - u_{0*}^{10} u_{c*}^{-9})^{1/2} \quad (19)$$

$$u_{c*} = \sqrt{u_{0*}^2 + 2x_*} \quad (20)$$

From Eqs.(3), (12), (15) and (17), Eqs.(21), (22) and (23) are also obtained for the developed region ($x_* \geq x_{1*}$).

$$x_* + c = \frac{h_{\infty*}}{a} \left\{ \frac{1}{2} \ln \frac{(h_* - h_{\infty*})^2}{h_*^2 + h_* h_{\infty*} + h_{\infty*}^2} + \sqrt{3} \tan^{-1} \frac{2h_* + h_{\infty*}}{-\sqrt{3}h_{\infty*}} \right\} \quad (21)$$

$$h_{\infty*} = \left\{ \frac{Re \alpha}{2 \left(1 - \frac{1}{3}\alpha \right)} \right\}^{1/3} \quad (22)$$

$$a = \frac{-24\alpha \left(1 - \frac{1}{3}\alpha \right)}{Re \left(\frac{4}{3}\alpha + \frac{1}{5}\alpha^2 \right)} \quad (23)$$

To obtain the film thickness h_* as a function of x_* , Re and θ , the inlet conditions, u_{0*} and h_{0*} , should be determined in advance by using the following Eqs.(24), (25), (26) and (27).

$$Q = u_0 h_0 \quad (24)$$

$$u_0 = \sqrt{2g \sin\theta h''} \quad (25)$$

$$h' - h_0 \cos\theta = h'' \quad (26)$$

$$h' = \left(\frac{Q}{317} \right)^{3/2} \quad (27)$$

Equation (27) is the Francis-Weir equation. The critical value x_{1*} is obtained from Eqs.(16), (19) and (20), with the value of which integration constant c in Eq.(21) is determined.

2. Results and Discussion

Some examples of $h_*(x_*)$, for $\alpha-1=0.0718$ and for $\alpha=1$, are shown in Fig. 2. α is not a sensitive parameter for film thickness when the value of x_* is small. The curves have maximum at $x_* \sim 10^2$ ($x \sim 1\text{cm}$). This fact agrees qualitatively with the observation that a falling film has a rising near the entrance. In Fig. 3, the variation of film thickness with Re at $x_* \sim 10^4$ is compared with the measurements⁵⁾ by the pointer

and gauge method.

Bruley¹⁾ solved numerically the momentum equation by the finite difference method for vertical falling films. His inlet condition coincides with that of this work for $\theta=90^\circ$, and he defined "entrance length" as the distance from the leading edge at which the surface velocity reached 99.99% of the terminal surface velocity. In Fig. 4, the "entrance lengths" estimated by both Bruley and the author are shown with the "initial length" at which a core region perishes ($c_* = 0$).

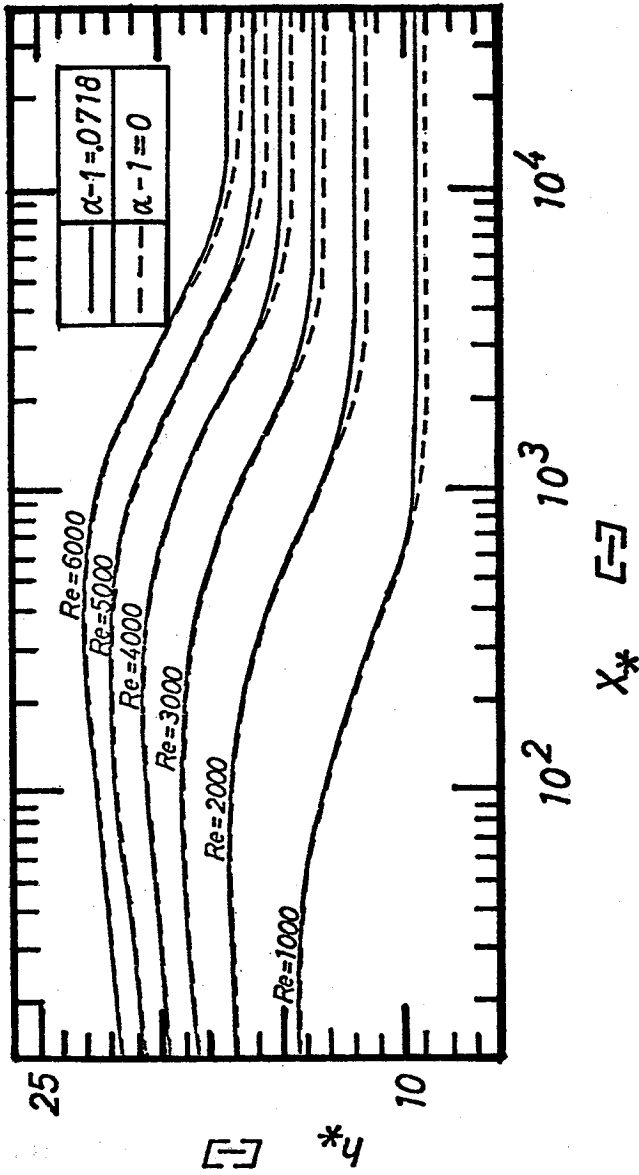


Fig. 2 Film thickness as function of x^* ($\theta = 8.9^\circ$)

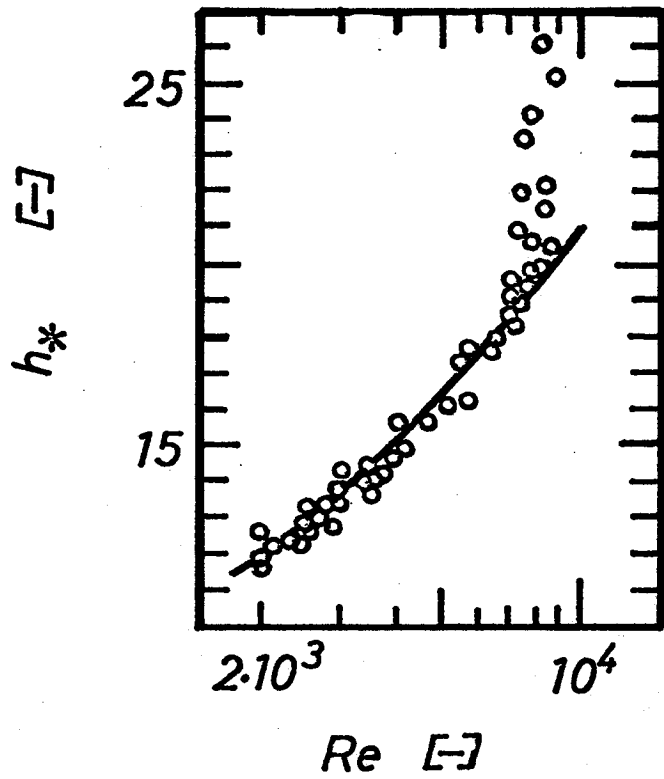


Fig. 3 Comparison of experimental and theoretical film thickness at $x=80\text{cm}$

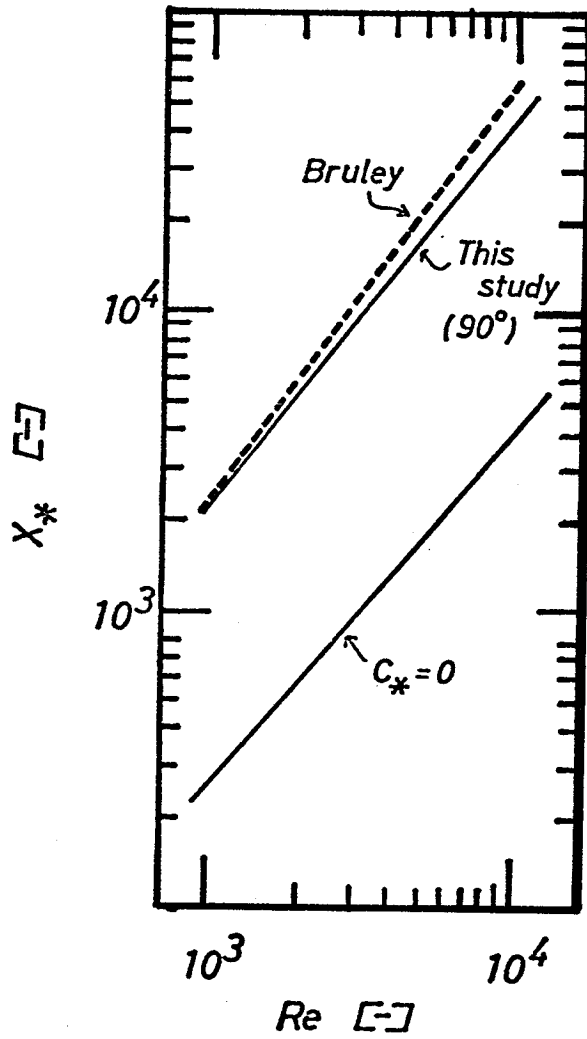


Fig. 4 Variations of initial length ($C_* = 0$) and entrance length

Conclusion

- 1) A flow model for falling liquid films has been put into the momentum integral equation to obtain the variation of film thickness. The results agree with the experiments.
- 2) "Entrance length" by the model shows the same tendency with that numerically analyzed by Bruley.

Nomenclature

c	= core region depth	[cm]
c_*	= $c(g \sin\theta)^{1/3}/\nu^{2/3}$	[-]
h	= film thickness	[cm]
h_*	= $h(g \sin\theta)^{1/3}/\nu^{2/3}$	[-]
$h_{\infty*}$	= terminal film thickness	[-]
K	= parameter defined by Eq.(5) in Chapter 2	[-]
Q	= $u \cdot h$	[cm ² /sec]
Re	= $4Q/\nu$	[-]
u	= fluid velocity	[cm/sec]
u_*	= $u/(\nu g \sin\theta)^{1/3}$	[-]
x	= distance from entrance	[cm]
x_*	= $x(g \sin\theta)^{1/3}/\nu^{2/3}$	[-]
y	= coordinate axis	[cm]
y_*	= $y(g \sin\theta)^{1/3}/\nu^{2/3}$	[-]
α	= parameter defined by Eq.(13)	[-]
δ	= boundary layer thickness	[cm]
δ_*	= $\delta(g \sin\theta)^{1/3}/\nu^{2/3}$	[-]
η	= y/h	[-]
θ	= inclination of plate to horizon	[deg]
ν	= kinematic viscosity of liquid	[cm ² /sec]
τ	= shear stress	[g/cm·sec ²]
τ_*	= $\tau/\rho(\nu g \sin\theta)^{2/3}$	[-]

<subscripts>

c = core region

o = entrance (x=0)

w = wall

l = position at $c_* = 0$

Literature cited

- 1) Bruley, D.F.: AIChE J., 11, 945(1965)
- 2) Cerro, R.L. and S. Whitaker: Chem. Eng. Sci.,
26, 785(1971)
- 3) Hassan, N.A.: Trans. ASME. Ser. E, 34, 535(1967)
- 4) Hangen, R.: ibid., 35, 631(1968)
- 5) Ito, R. and K. Tomura: J. Chem. Eng. Japan,
12, 10(1979)
- 6) Murthy, V.N. and P.K. Sarma: Chem. Eng. Sci.,
32, 566(1977)
- 7) Stüchel, A. and M.N. Özisik: ibid., 31,
369(1976)
- 8) Whitaker, S. and R.L. Cerro: ibid., 29, 963(1974)

CHAPTER 4

WAVE INCEPTION

Abstract

Transition from calming to rippling, the so-called wave inception has been measured photographically at the flow rate $Re=500-10000$ and inclination angles $\theta=9^\circ-52^\circ$, and analyzed based on the momentum integral equation. At the critical position of wave inception, the thickness and its gradient of film, or the balance of gravitational force and surface tension, may play an important role in wave inception. The measurements of wave inception for inclined plates and the available data for vertical wall agree with the analysis.

Introduction

Falling liquid films on inclined plates and on vertical wall have many applications to heat and mass transfer equipments. These transfer rates are intensively influenced by the surface behavior of falling liquid films, by rippling motion^{8,20,26)} and by turbulent flow conditions⁷⁾. Films on vertical wall have "calming zone" without wave motion for a short distance below the liquid distributor^{18,22,23,25,26)}. On the other hand, it is pointed out in Chapter 2 that the length of "calming zone" on an inclined plate is rather long. The dependence of wave inception on Re and/or inclination angle has not been investigated systematically. A few experimental work^{4,18,22)} on vertically falling films were reported, but no reasonable explanations have been made yet.

Some reports suggest the importance of understanding the mechanism of wave inception to the problems of mass transfer^{8,26)} and the characteristics^{15,19,23)} of falling liquid films.

The wave inception under various Reynolds numbers and inclination angles of the plate is observed and analyzed based on the integral

equation of motion.

1. Observation

The experimental apparatus is described in detail in Chapter 2. Deionized water was falling on the inclined plate (16.5cm wide, 160cm long) and the surfaces were photographed to clarify the disturbed surface. Liquid flow rates were ranged from $Re=500$ to 10000, and the inclination angles of the plate were 9° , 33° and 52° , and all runs were carried out under no air flow conditions.

The characteristics of film surface through the whole runs are as follows;

- (1) "Calming zone" exists for a certain distance from the distributor and the inception of wave motion sets in at "the line of wave inception" and rippling waves progress down the plate and gradually lose their regularity.
- (2) The wave length at the line of wave inception decreases as flow rate increases
- (3) $Re>6000$, turbulent spots occurred randomly

sometimes and somewhere to disturb the surface. The distance from the distributor to the line of wave inception does neither increase nor decrease monotonously with the liquid flow rate, as shown in Fig. 3.

2. Analysis

The equation of motion for the flow shown in Fig. 1 is simplified as

$$\begin{aligned}
 -\frac{d}{dx_*} \int_0^{h_*} u_*^2 dy_* + h_* + u_{s*} \frac{d}{dx_*} \int_0^{h_*} u_* dy_* \\
 = \tau_{w*} - \tau_{s*}
 \end{aligned}
 \tag{1}$$

and analytically solved with the velocity profile given in the previous chapter, which consists of two regions, initial region (with core flow) and developed region (no core, $\partial/\partial x \neq 0$). The deviation from Nusselt's analysis is indicated by α , that is obtained experimentally as 1.0718.

$$(\tau_{w*} - \tau_{s*}) / \tau_{w*} \equiv \alpha
 \tag{2}$$

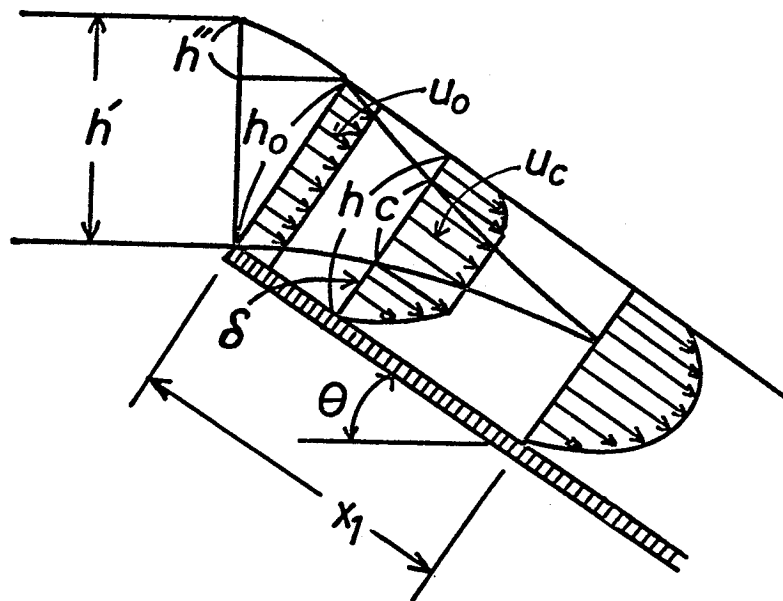


Fig. 1 Flow model

By use of Eqs.(24)~(27) in Chapter 3, initial film thickness h_0 can be estimated as follows

$$h_{0*}^3 \cos\theta - h_{0*}^2 \frac{(g \sin\theta)^{1/3} \text{Re}^{3/2}}{\sqrt{5/6} \cdot 1411} + \text{Re}^2 = 0 \quad (3)$$

For the developed region, Eq.(4) is derived.

$$x_* + C_i = \frac{h_{\infty*}}{a} \left\{ \frac{1}{2} \ln \frac{(h_* - h_{\infty*})^2}{h_*^2 + h_* h_{\infty*} + h_{\infty*}^2} + \sqrt{3} \tan^{-1} \frac{-2h_* + h_{\infty*}}{-\sqrt{3} h_{\infty*}} \right\} \quad (4)$$

where

$$h_{\infty*} = \left\{ \frac{\text{Re} \alpha}{2(1 - \frac{1}{3} \alpha)} \right\}^{1/3}$$

$$a = \frac{-24\alpha(1 - \frac{1}{3} \alpha)}{\text{Re} (\frac{4}{3} - \alpha + \frac{1}{5} \alpha^2)}$$

$$u_{s*} = \frac{(2 - \alpha)\text{Re}}{4(1 - \frac{1}{3} \alpha) h_*} \quad (5)$$

It is noted that the integral constant C_i in Eq.(4) depends on the value of h_{0*} .

3. Results and Discussion

The film thickness h_{c*} at the wave inception can be obtained from Eqs.(3) and (4). However, it is difficult to get accurate values of h_{c*} , when Re and θ are small, because the value of dh_*/dx_* at $x_*=x_{c*}$ becomes very small. In Fig. 2, h_{c*} calculated for x_{c*} observed is shown in the form of z_* vs. Re , which is independent of θ and correlated by Eq.(7)

$$z_* \equiv h_{c*} - h_{\infty*} \quad (6)$$

$$z_* = 7.505 \cdot 10^{-24} \cdot Re^{5.807} \quad (7)$$

$$(r = 0.975)$$

where, r stands for the coefficient of correlation. Inversely, x_{c*} can be estimated with Eqs.(4) and (7). The examples are shown in Fig. 3 with the observed values for 9° inclined plate and with the available data^{18,22,26)} for vertical wall. Though, the observed values for $\theta=9^\circ$ have been excluded in derivation of the correlation Eq.(7), because the accuracy of h_{c*} is low, the agreements of the observed values with the calculated values are very good. In Fig. 3, the data for 33° are excluded, because these have been used to

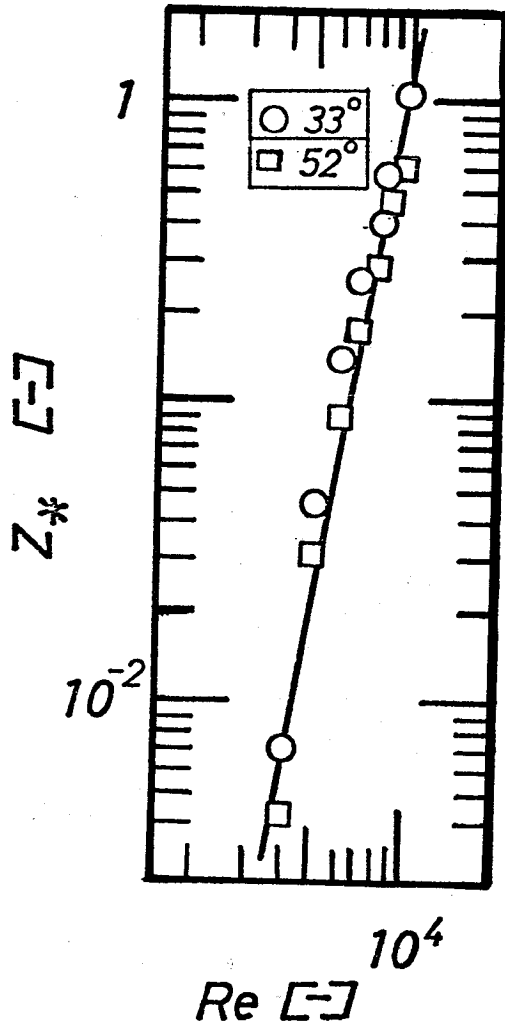


Fig. 2 Film thickness z_* at wave inception

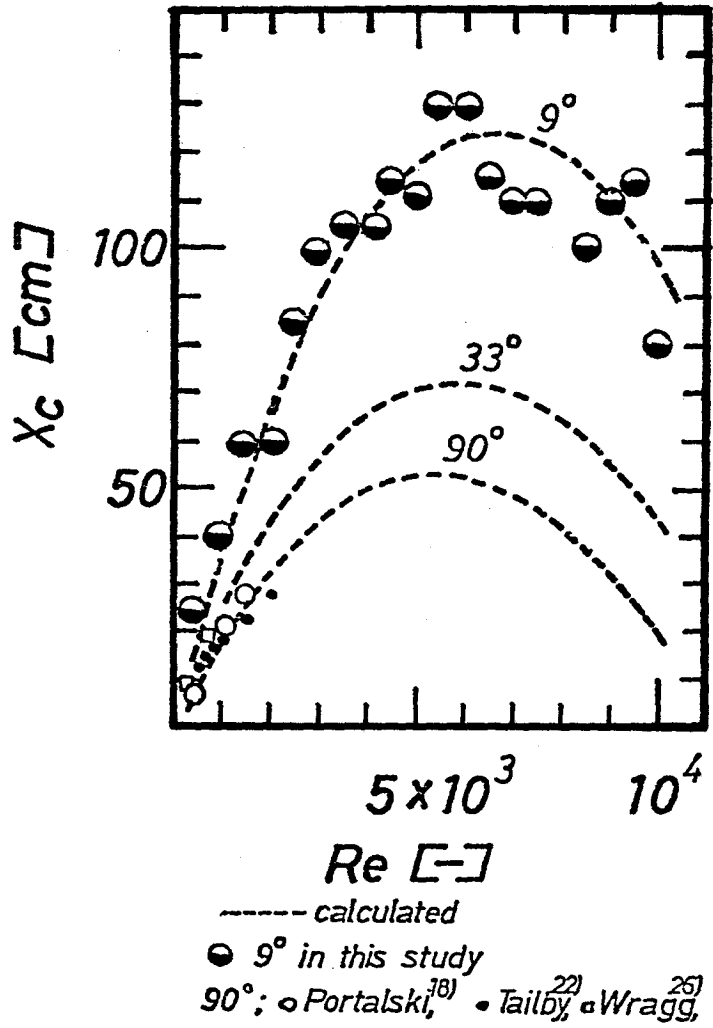


Fig. 3 Positions of wave inception

obtain the correlation Eq.(7).

The positions of wave inception has been expressed successfully. The following is the discussion on the characteristics of flow at the wave inception based on the flow model. Almost all of the stability theories^{1,3,9,16)} were concerned with fully developed flow and concluded that the falling films were almost always unstable at Re rather less than about 10. It is natural that the theories can not explain the occurrence of wave inception in developing region.

A few investigators studied the stability of the developing laminar flow in parallel-plate channel⁶⁾ and in pipe^{12,24)} but could not explain the experimental results.

According to the hydraulic jump theory, the critical flow arises under the following condition

$$\frac{dE_{sp*}}{dh_*} = 0 \quad (8)$$

E_{sp} is called the specific energy, and derived for the flow model considered in this chapter as

$$E_{sp*} \equiv h_* + \frac{\bar{u}_*^2}{2} = h_* + \frac{Re^2}{32h_*^2} \quad (9)$$

Eq.(9) gives

$$Fr \equiv \frac{Re^2}{16h_*^3} = 1 \quad (10)$$

Under the condition of this work, Froude number is always much greater than unity, then the flow is supercritical everywhere. The theory of hydraulic jump can not explain the wave inception. The reason of this failure seems to be caused by the surface tension effect being neglected.

From Eq.(4), $\frac{dh_*}{dx_*}$ is derived as

$$\frac{dh_*}{dx_*} = \frac{8(1 - \frac{1}{3} \alpha)}{Re(\frac{4}{3} - \alpha + \frac{1}{5} \alpha^2)} \left\{ \alpha - \frac{2(1 - \frac{1}{3} \alpha)}{Re} h_*^3 \right\} \quad (11)$$

The radius of surface curvature R_* at the wave inception x_{c*} is obtained.

$$R_* = \frac{[1 + (\frac{dh_*}{dx_*})^2]^{1.5}}{\frac{d^2h_*}{dx_*^2}} \quad (12)$$

In Fig. 4, z_* and $-\frac{dh_*}{dx_*} \Big|_{x_*=x_{c*}}$ are plotted and correlated as follows;

$$-\frac{dh_*}{dx_*} \Big|_{x_{c*}} = 5.976 \cdot 10^{-22} \cdot z_*^{0.763} \quad (13)$$

(r = 0.999)

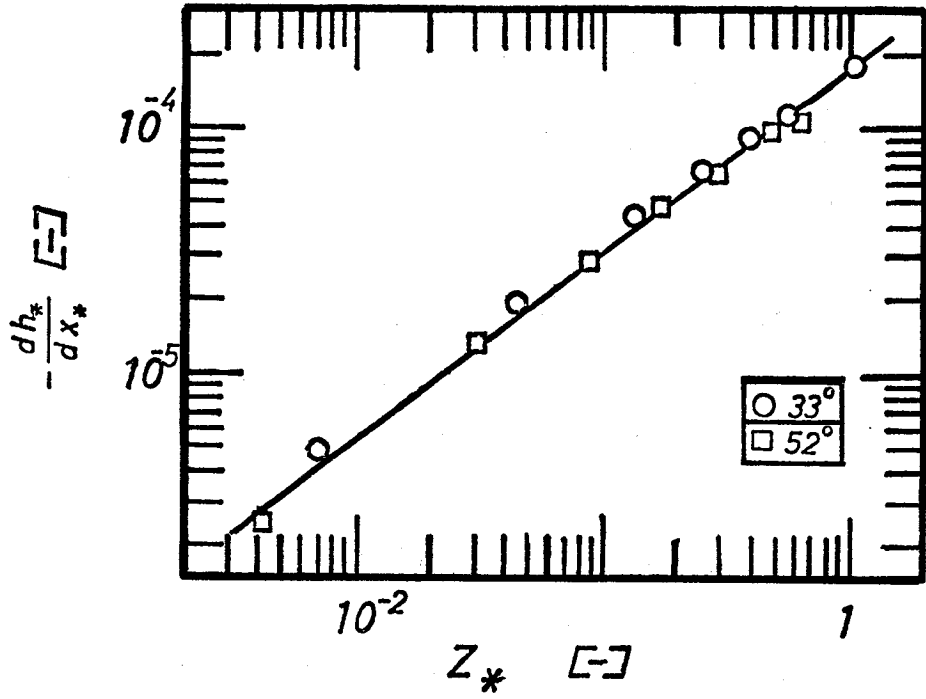


Fig. 4 Surface gradient vs. Film thickness at wave inception

In Fig. 5, $1/R_*$, corresponding to surface tension force, vs. z_* , gravity force, are plotted and the correlation is obtained as

$$1/R_* = 3.39 \cdot 10^{-8} \cdot z_*^{0.555} \quad (14)$$

$$(r = 0.990)$$

Clearly the wave inception is influenced by the shape of the film surface, and seems to be the position at which surface tension force becomes to be incapable of supporting the weight of z . And any disturbance at wave inception does not propagate upstream because the flow is supercritical everywhere ($Fr > 1$).

The flow inlet conditions influence the shape of $x_{c*}(Re, \theta)$, because C_i in Eq.(4) depends on h_{0*} . In Fig. 6, h_{0*} vs Re and θ are given. Stüchel and Özisik²¹⁾ derived the function $h_*(x_*)$ analytically, however did not show explicitly the inlet condition but treated it as parameter $\beta \equiv h_0/h_\infty$. Their results showed $h_*(x_*)$ depending much on β .

"Initial region" and "entrance region" have been defined in the previous chapter. In Fig. 7, the "initial region" and "entrance region" compared with the position of wave inception are shown. It is clear that the wave inception occurs in the developed zone.

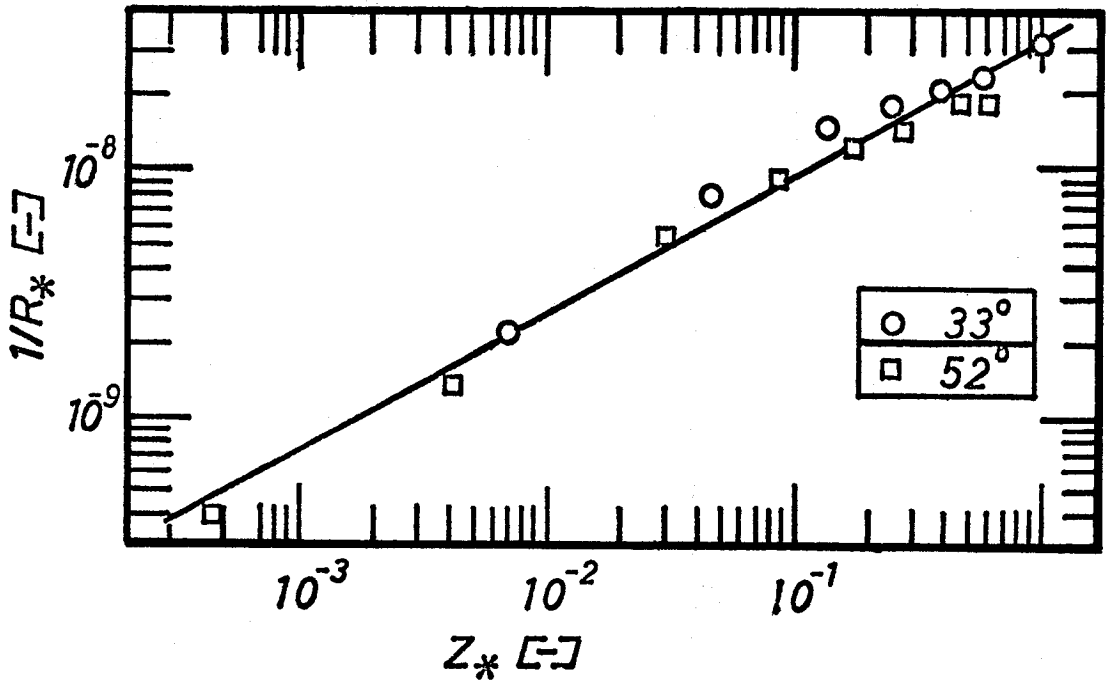


Fig. 5 $1/R_*$ vs. z_* at wave inception

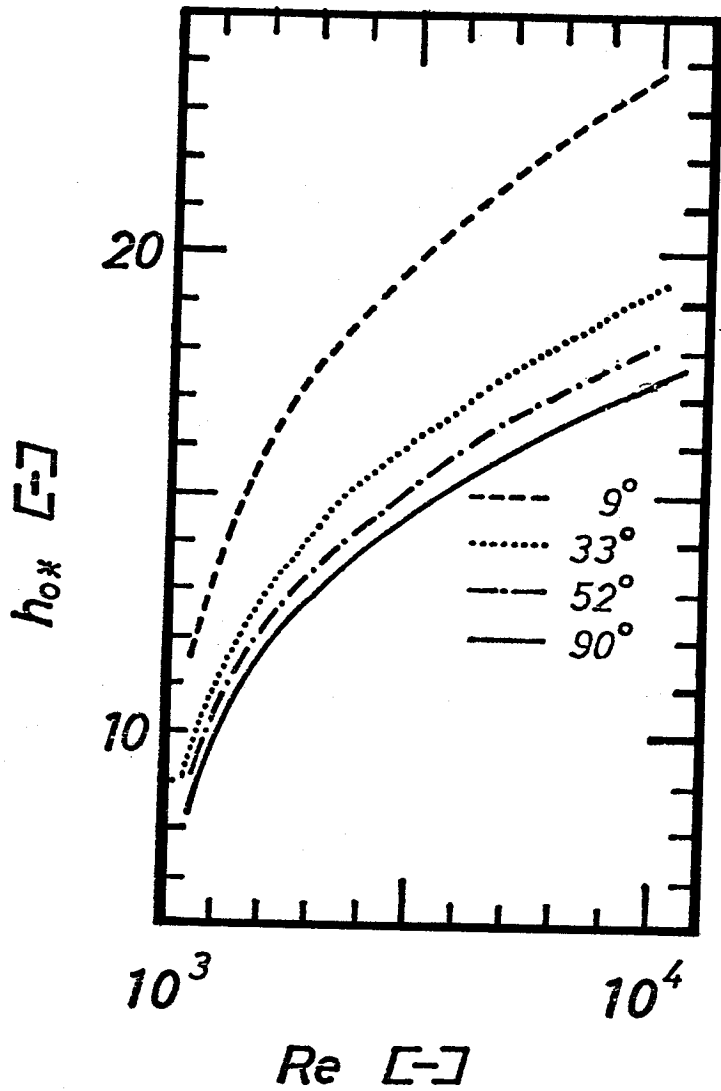


Fig. 6 Initial film thickness vs. Re

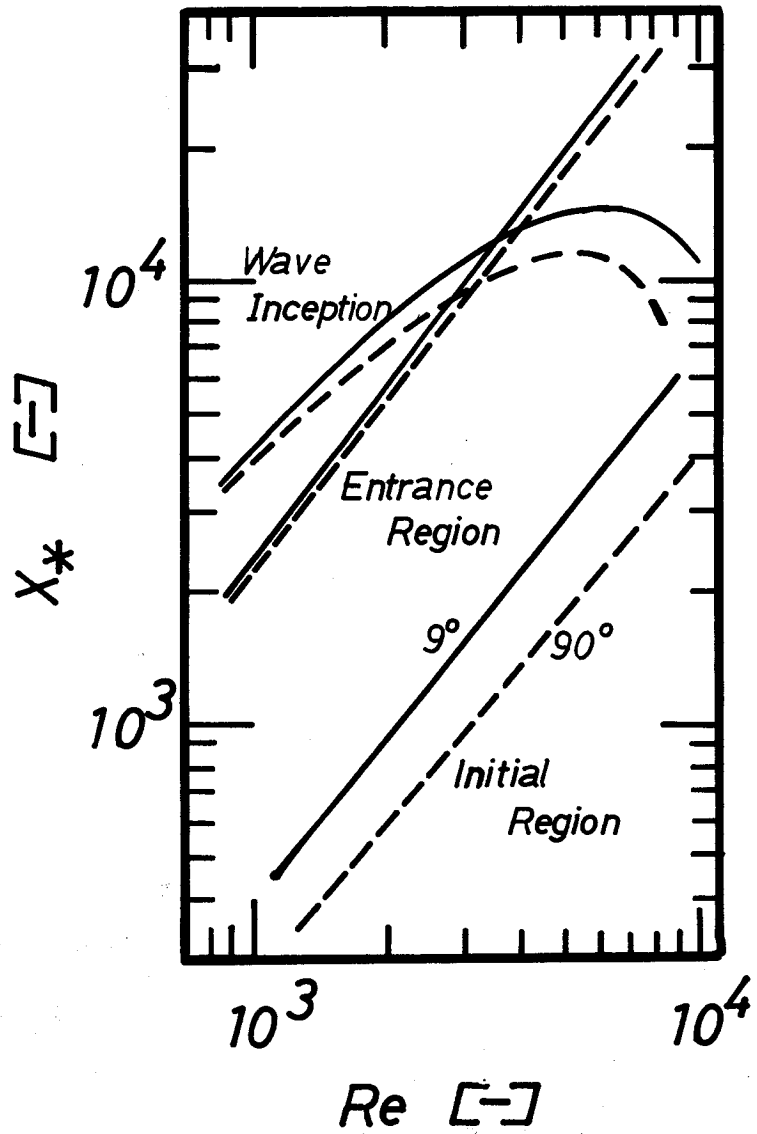


Fig. 7 Initial region, entrance region and the position of wave inception

Conclusion

(1) Observation of the surface behavior of falling liquid film on inclined plates has been made with the special attention to x_{c*} above which no wave motion appeared. At x_{c*} , wave inception took place and wave motion progressed downstream gradually losing their regularity.

(2) The location x_{c*} is analyzed based on the integral equation of motion, and predicted with Eqs.(4) and (7).

(i) The calculated values agree very well with the observed values for films on both inclined plates and vertical walls.

(ii) The films under the experimental conditions are supercritical ($Fr > 1$).

(iii) The analysis suggests that the wave inception is influenced by the shape of the film surface, that is, by the thickness of film and its gradient in the flow direction at the wave inception. It may be considered that the balance of gravitational force and surface tension plays an important role in the wave inception.

Nomenclature

C	= core region depth	[cm]
C_i	= integral constant in Eq.(4)	[-]
E_{sp}	= specific energy	[cm]
E_{sp*}	= $E_{sp}(g \sin\theta)^{1/3}/\nu^{2/3}$	[-]
Fr	= Froude number	[-]
h	= liquid film thickness	[cm]
h_*	= $h(g \sin\theta)^{1/3}/\nu^{2/3}$	[-]
Q	= $\bar{u} \cdot h$	[cm ² /sec]
R	= radius of surface curvature	[cm]
R_*	= $R(g \sin\theta)^{1/3}/\nu^{2/3}$	[-]
Re	= $4Q/\nu$	[-]
u	= fluid velocity	[cm/sec]
u_*	= $u/(\nu g \sin\theta)^{1/3}$	[-]
\bar{u}	= average fluid velocity	[cm/sec]
x	= distance from entrance	[cm]
x_*	= $x(g \sin\theta)^{1/3}/\nu^{2/3}$	[-]
z	= $h_c - h_\infty$	[cm]
z_*	= $z(g \sin\theta)^{1/3}/\nu^{2/3}$	[-]
α	= parameter defined by Eq.(2)	[-]
θ	= inclination of plate to horizon	[deg]
ν	= kinematic viscosity of liquid	[cm ² /sec]

$$\begin{aligned} \tau &= \text{shear stress} && [\text{g/cm}\cdot\text{sec}^2] \\ \tau_* &= \tau/\rho(vg \sin\theta)^{2/3} && [-] \end{aligned}$$

<Subscripts>

- c = at wave inception
- o = at entrance (x=0)
- s = at air-liquid surface
- w = at wall
- ∞ = at infinitive (x= ∞)

Literature Cited

- 1) Anshus, B.E. and S.L. Goren: AIChE J., 12,
1005(1966)
- 2) Bruley, D.F.: *ibid.*, 11, 945(1965)
- 3) Benjamin, T.B.: J. Fluid Mech., 2, 554(1957)
- 4) Cerro, R.L. and S. Whitaker: Chem. Eng. Sci.,
26, 742(1971)
- 5) Cerro, R.L. and S. Whitaker: *ibid.*, 26,
785(1971)
- 6) Chen, T.S. and E.M. Sparrow: J. Fluid Mech.,
30, 209(1967)
- 7) Davies, J.T. and A.M. Shawk: Chem. Eng. Sci.,
29, 1801(1974)
- 8) Einarsson, A. and A.A. Wragg: *ibid.*, 26,
1289(1971)
- 9) Hanratty, T.J. and A. Hershman: AIChE J.,
7, 488(1961)
- 10) Hassan N.A.: Trans. ASME Ser. E, 34, 535(1967)
- 11) Haugen, R.: *ibid.*, 35, 631(1968)
- 12) Huang, L.M. and T.S. Chen: Phys. Fluids, 17,
245(1974)
- 13) Ito, R. and K. Tomura: J. Chem. Eng. Japan,
12, 10(1979)

- 14) Ito, R. and K. Tomura: J. Chem. Eng. Japan,
12, 66(1979)
- 15) Jones, L.O. and S. Whitaker: AIChE J., 12,
525(1966)
- 16) Krantz, W.B. and S.L. Goren: Ind. Eng. Chem.
Fundam., 10, 91(1971)
- 17) Murthy, V.N. and P.K. Sarma: Chem. Eng. Sci.,
32, 566(1977)
- 18) Portalski, S. and A.J. Clegg: *ibid.*, 27,
1257(1972)
- 19) Shiotsuka, T., N. Honda and Y. Ohata: Kagaku
Kōgaku, 21, 703(1957)
- 20) Stainthorp, F.P. and G.J. Wild: Chem. Eng. Sci.,
22, 701(1967)
- 21) Stüchel, A. and M.N. Özisik: *ibid.*, 31,
369(1976)
- 22) Tailby, S.R. and S. Portalski: *ibid.*, 17,
283(1962)
- 23) Tailby, S.R. and S. Portalski: Trans. Instn.
Chem. Engrs., 40, 114(1962)
- 24) Tatsumi, T.: J. Phys. Soc. Japan, 7, 495(1952)
- 25) Wilkes, J.O. and R.M. Nedderman: Chem. Eng. Sci.,
17, 177(1962)
- 26) Wragg, A.A. and A. Einarsson: *ibid.*, 25,
67(1970)

CHAPTER 5

SIMULTANEOUS MEASUREMENTS OF THICKNESS AND LOCAL MASS TRANSFER RATE IN RIPPLING ZONE

Abstract

It is well known that wave motion on falling liquid films influences the mass transfer rates, however, the previous reports were limited to the time averaged values.

Simultaneous measurements of instantaneous mass transfer rate and film thickness are made. The relation of mass transfer rate to film thickness shows a hysteresis, and a peak of mass transfer rate precedes the corresponding one of film thickness, and the phase shift is estimated as 16% of the period.

Introduction

Falling liquid films have many applications in industry, especially the rate of mass transfer is essential for the design of many equipments.

Wave motions, which appear in downstream after the position of wave inception on films, significantly enhance mass transfer rates⁴⁾. Many studies on mass transfer both through the gas-liquid and the solid-liquid interfaces of wavy liquid flow under various conditions, have been made experimentally^{2,4,7,9,15)} and theoretically^{1,5,6,10,12)}.

However, the investigations dealt with the time averaged values.

Instantaneous measurements of local liquid-solid mass transfer^{3,14)} and simultaneous measurements of wave amplitude and local mean concentration¹¹⁾ and ones of wall shear stress and film thickness⁸⁾ have been previously reported.

Instantaneous film thickness and local liquid-solid mass transfer rate have been measured simultaneously. And the relations between them will be discussed.

1. Experimental Apparatus and Method

The test section was 25cm wide and 300cm long, and the surface was almost entirely covered with a nickel plate and inclined 9° to the horizon. Measuring the electrical resistance between two parallel nickel wires of 0.15mm in diameter and 1.8mm apart which pierced through the film as shown in Fig. 1, the author obtained the instantaneous film thickness. An electrochemical technique, the cathodic reduction of ferricyanide ions at small nickel electrode, was used to measure the local instantaneous mass transfer rate. The isolated cathode, 1mm in diameter, insulated from the surrounding nickel plate, was located at 180cm downstream from the liquid distributor. The reliances of these techniques have been confirmed by many workers^{3,8,13,14,15}). The experimentals have been carries out in rippling zone in the range of Re 400~1200.

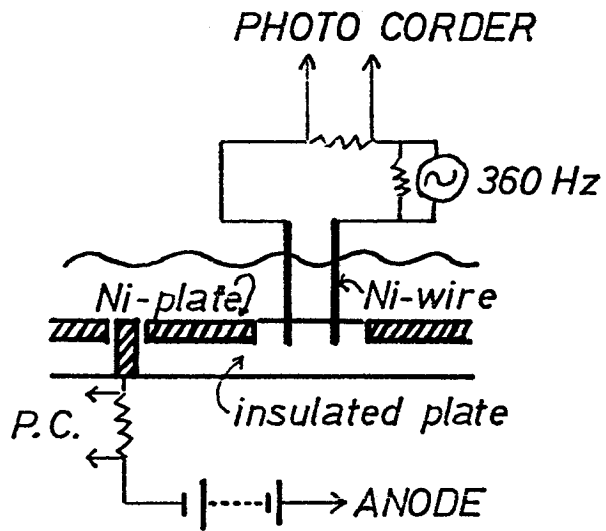


Fig. 1 Sketch of measuring system

2. Results and Discussion

It is difficult to define the periods both of a wave motion and a mass transfer rate, as pointed out by Tells and Dukler¹³⁾ and Wragg and Einarsson¹⁴⁾. Typical measurements of k and h are shown in Fig. 2. The shapes of these two waves are very complicated and different each other. Although the dependency of k on h is not so simple, distinct time lag between peaks of k and h can be seen for all runs.

Sets of k_* and h_* measured at the same time are related with each other in Fig. 3, and circulate clock-wisely showing a hysteresis. The center and the shape of the circulation vary at random with the individual wave.

Two dimensionless groups H and K are introduced to unify the individual circle.

$$H \equiv \frac{h_{\max*} - h_{\min*}}{h_*} \quad (1)$$

where

$$h_* = h_{\min*} + (h_{\max*} - h_{\min*}) / 2$$

$$K \equiv \frac{k_{\max*} - k_{\min*}}{k_*} \quad (2)$$

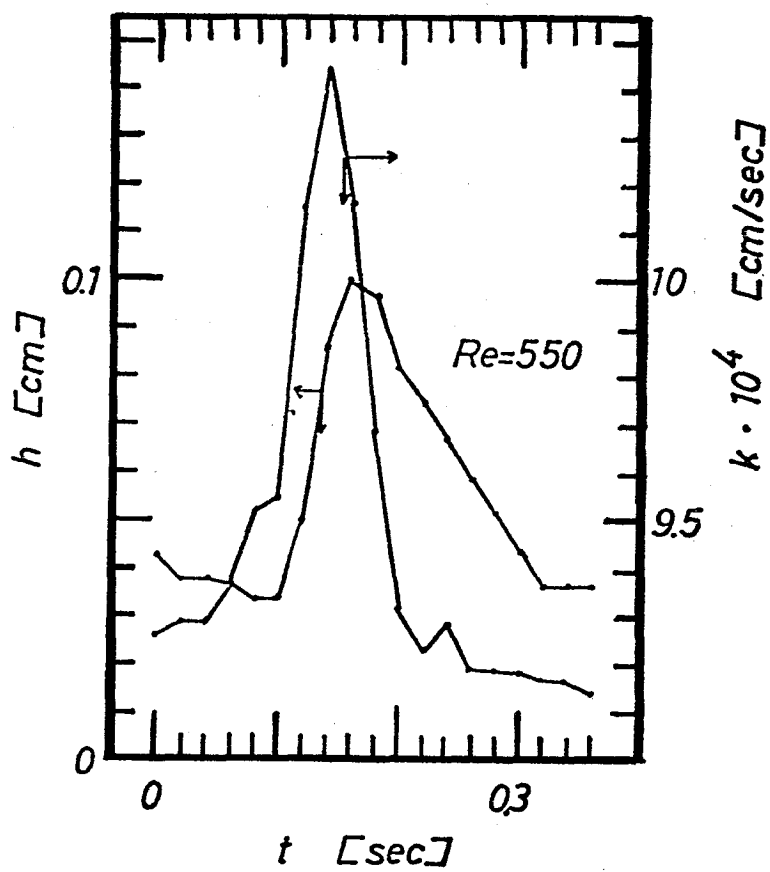


Fig. 2 Film thickness and liquid-solid mass transfer coefficient

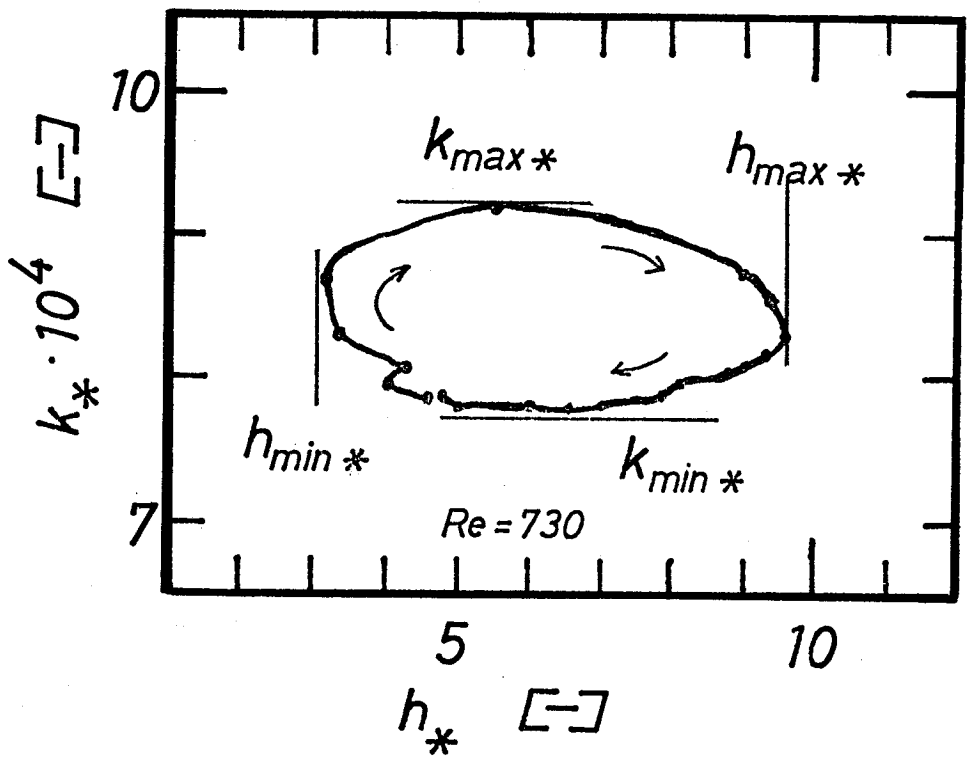


Fig. 3 A circle of k_* and h_*

where

$$k_* = k_{\min*} + (k_{\max*} - k_{\min*}) / 2$$

H and K are correlated by the following equations as shown in Fig. 4.

$$H = 1.43 \cdot 10^{-3} \cdot \text{Re} \quad (3)$$

$$K = 2.63 \cdot 10^{-4} \cdot \text{Re} \quad (4)$$

An individual circle can be normalized in the form of H_i and K_i .

$$H_i = \frac{\frac{h_*}{\bar{h}_*} - 1}{H/2} \quad (5)$$

$$K_i = \frac{\frac{k_*}{\bar{k}_*} - 1}{K/2} \quad (6)$$

An example is given in Fig. 5. If the circle for each wave is expressed with phase shift β , as

$$\cos^2 2\pi\beta - 2H_i K_i \cos 2\pi\beta - 1 + H_i^2 + K_i^2 = 0 \quad (7)$$

Then, β can be estimated by

$$\cos 2\pi\beta = \frac{1}{n_i} \sum_{i=1}^n (H_i K_i + \sqrt{H_i^2 K_i^2 - H_i^2 - K_i^2 + 1}) \quad (8)$$

Stainthorp and Wild¹¹⁾ measured the film thick-

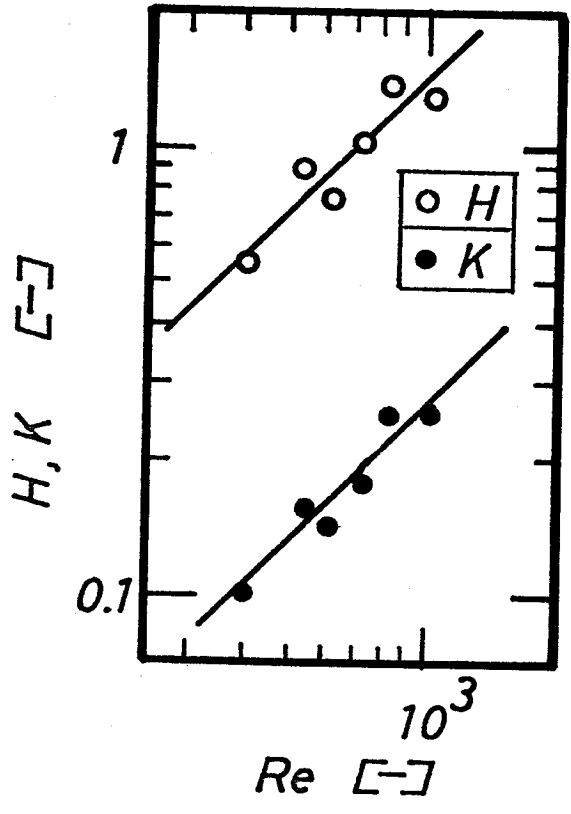


Fig. 4 Dependence of H and K on Re

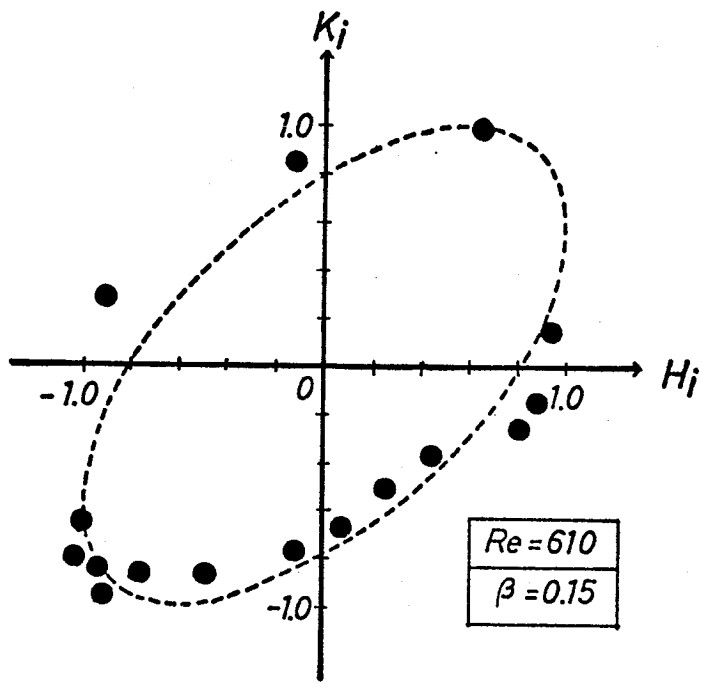


Fig. 5 K_i vs H_i

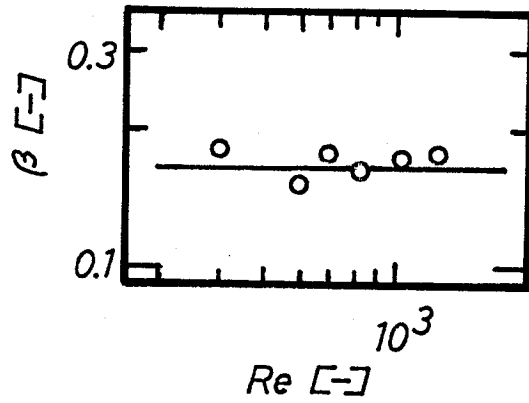


Fig. 6 Dependence of β on Re

ness and local mean concentration simultaneously, by use of an optical system, and observed the peak of mean concentration leading the corresponding one of physical wave. And they suggested a flow pattern inside a wave, but further work will be necessary.

Conclusion

- (1) Instantaneous local mass transfer rate and film thickness of falling liquid flow on an inclined plate have been measured simultaneously.
- (2) Instantaneous local mass transfer and film thickness show a hysteresis.
- (3) A distinct time lag between peaks of mass transfer rate and film thickness has been observed, and the phase shift is estimated as 16% of the period.

Nomenclature

H	= parameter defined by Eq.(1)	[-]
H_i	= parameter defined by Eq.(5)	[-]
h	= film thickness	[cm]
h_*	= $h (g \sin\theta)^{1/3} / \nu^{2/3}$	[-]
K	= parameter defined by Eq.(2)	[-]
K_i	= parameter defined by Eq.(6)	[-]
k	= local liquid-solid mass transfer coefficient	[cm/sec]
k_*	= $k / (\nu g \sin\theta)^{1/3}$	[-]
n	= number of data	
Re	= Reynolds number ($4Q/\nu$)	[-]
β	= phase shift defined by Eq.(7)	[-]
θ	= inclination of plate to horizon	[deg]
ν	= kinematic viscosity of liquid	[cm ² /sec]

Literature Cited

- 1) Banerjee, S., E. Rhodes and D.S. Scott: Chem. Eng. Sci., 22, 43(1967)
- 2) Ciborowski, J.W. and R.M. Rychlicki: Int. J. Heat Mass Transfer, 14, 1261(1971)
- 3) Einarsson, A. and A.A. Wragg: Chem. Eng. Sci., 26, 1289(1971)
- 4) Goren, S.L. and R.V.S. Mani: AIChE J., 14, 57(1968)
- 5) Howard, D.W. and E.N. Lightfoot: *ibid.*, 14, 458(1968)
- 6) Javdani, K.: Chem. Eng. Sci., 29, 61(1974)
- 7) Kramers, H. and P.J. Kreyger: *ibid.*, 6, 42(1956)
- 8) Miya, M., D. Woodmansee and T.J. Hanratty: *ibid.*, 26, 1915(1971)
- 9) Oliver, D.R. and T.E. Atherinos: *ibid.*, 23, 525(1968)
- 10) Ruckenstein, E. and C. Berbente: Int. J. Heat Mass Transfer, 11, 743(1968)
- 11) Stainthorp, F.P. and G.J. Wild: Chem. Eng. Sci., 22, 701(1967)

- 12) Tamir, A. and Y. Taitel: Chem. Eng. Sci., 26,
799(1971)
- 13) Telles, A.S. and A.E. Dukler: Ind. Eng. Chem.
Fundam., 9, 412(1970)
- 14) Wragg, A.A. and A. Einarsson: Chem. Eng. Sci.,
25, 67(1970)
- 15) Wragg, A.A., P. Serafimidis and A. Einarsson:
Int. J. Heat Mass Transfer, 11, 1287(1968)

CHAPTER 6

SUMMARY

- 1] Surface behaviors of falling liquid films on inclined plates have been observed in the range of Re 400-20000.
 - (1) The flow behavior is classified into three zones, that is, calming, rippling and turbulent zones.
 - (2) "Calming zone" exists near the inlet and is followed by "rippling zone", which gradually loses the regularity of shape of wave and changes into "turbulent zone" in a film.
 - (3) The length of calming zone varies complicatedly with Re and θ . For $Re < 2000$ and $Re > 10000$, calming zone is very short. However, for the intermediate range of Re , calming zone is observed for long distance. In other words, at a fixed point calming zone appears at

higher Re than does rippling zone.

2] Velocity profile in calming zone has been measured by use of the hydrogen bubble method and it is found that

(1) the flow is laminar with the drag of air at liquid surface, in spite of $2000 < Re < 6000$, and

(2) the film thickness and flow rate estimated by the velocity profile coincide with the measurements.

3] A flow model in calming zone has been confirmed by comparing the estimations of film thickness with the measurements at a fixed point. And the model has been utilized to calculate the lengths of entrance and initial zones.

4] Based on the flow model, the critical positions of wave inception for films both on vertical walls and inclined plates have been successfully expressed.

(1) The length of calming zone increases with increasing Re and then decreases, that is, the length has a maximum at $Re \sim 6000$. And at a fixed Re , the length increases as θ decreases.

(2) Wave inception occurs in the developed zone

without core region.

(3) The balance of gravitational force and surface tension force, and the inlet condition play a role in wave inception.

5] Simultaneous measurements of instantaneous film thickness and local mass transfer rate in rippling zone show a histerisis.

Velocity Profile measurements

Re=2600

x=67cm

$\theta=17.2^\circ$

T=24.0°C

P.I.=8.09ms

u [cm/sec]	32.5	52.1	68.6	78.7
y/h [-]	0.2	0.3	0.4	0.5

86.8	92.8	96.9	99.5	102
0.6	0.7	0.8	0.9	1.0

Re=3200

x=115cm

$\theta=9.9^\circ$

T=26.0°C

P.I.=9.17ms

u	37.8	51.8	63.2	74.3
y/h	0.2	0.3	0.4	0.5

83.2	88.2	90.3	92.5	93.2
0.6	0.7	0.8	0.9	1.0

Re=3200

x=67cm

$\theta=17.2^\circ$

T=24.0°C

P.I.=6.23ms

u	44.8	64.0	77.4	89.3
y/h	0.2	0.3	0.4	0.5

100	110	117	119	120
0.6	0.7	0.8	0.9	1.0

(Velocity Profile)

Re=3500

x=67cm

$\theta=7.4^\circ$

T=26.5°C

P.I.=9.18ms

u [cm/sec]	42.9	51.9	58.9	65.8
y/h [-]	0.2	0.3	0.4	0.5

73.3	80.4	85.4	87.0	87.1
0.6	0.7	0.8	0.9	1.0

Re=4000

x=67cm

$\theta=7.4^\circ$

T=26.3°C

P.I.=6.15ms

u	44.7	56.6	64.0	74.3
y/h	0.2	0.3	0.4	0.5

83.2	91.0	96.2	96.8	97.0
0.6	0.7	0.8	0.9	1.0

Re=4000

x=67cm

$\theta=7.4^\circ$

T=23.6°C

P.I.=5.40ms

u	42.2	59.7	72.4	84.0
y/h	0.2	0.3	0.4	0.5

92.5	99.5	104	106	109
0.6	0.7	0.8	0.9	1.0

(Velocity Profile)

Re=4000

x=67cm

$\theta=7.4^\circ$

T=23.7°C

P.I.=5.40ms

u [cm/sec]	43.5	60.0	72.3	84.2
y/h [-]	0.2	0.3	0.4	0.5

92.2	101	107	109	108
0.6	0.7	0.8	0.9	1.0

Re=4000

x=67cm

$\theta=7.4^\circ$

T=23.8°C

P.I.=5.41ms

u	43.8	58.0	70.9	83.6
y/h	0.2	0.3	0.4	0.5

94.1	103	107	109	108
0.6	0.7	0.8	0.9	1.0

Re=4600

x=67cm

$\theta=7.4^\circ$

T=23.6°C

P.I.=6.45ms

u	46.2	58.8	72.2	85.4
y/h	0.2	0.3	0.4	0.5

90.7	96.2	108	109	110
0.6	0.7	0.8	0.9	1.0

(Velocity Profile)

Re=4700

x=67cm

$\theta=7.4^\circ$

T=23.4°C

P.I.=5.40ms

u [cm/sec]	48.9	62.7	77.7	91.0
y/h [-]	0.2	0.3	0.4	0.5

103	110	116	119	121
0.6	0.7	0.8	0.9	1.0

Re=4900

x=67cm

$\theta=7.4^\circ$

T=23.4°C

P.I.=5.40ms

u	44.5	62.6	77.2	91.2
y/h	0.2	0.3	0.4	0.5

103	110	115	118	117
0.6	0.7	0.8	0.9	1.0

Re=5000

x=67cm

$\theta=7.4^\circ$

T=23.4°C

P.I.=5.40ms

u	46.6	63.7	79.5	92.5
y/h	0.2	0.3	0.4	0.5

103	112	117	120	122
0.6	0.7	0.8	0.9	1.0

(Velocity Profile)

Re=6100

x=67cm

$\theta=7.4^\circ$

T=22.9°C

P.I.=5.41ms

u[cm/sec]	54.2	72.6	88.9	103
y/h [-]	0.2	0.3	0.4	0.5

113	120	124	127	128
0.6	0.7	0.8	0.9	1.0

Film Thickness by Pointer and Gauge ($\theta=8.9^\circ$)

Re · 10 ⁻³ [-]	4.86	5.32	5.98	6.44	6.97	7.36
T [°C]	14.3	14.4	14.4	14.5	14.6	14.7
h [mm]	1.52	1.55	1.64	1.70	1.78	1.81

7.70	8.14	8.49	6.81	7.83	8.50	9.11	9.72
14.7	14.8	14.8	15.1	15.1	15.2	15.3	15.4
1.87	1.91	1.97	1.86	1.97	2.12	2.38	2.88

10.3	11.0	11.7	12.2	12.7	12.2	3.22	3.04
15.5	15.6	15.7	15.7	15.8	14.2	11.9	12.0
2.99	3.35	3.46	3.51	3.60	3.64	1.39	1.35

2.80	2.57	2.35	2.14	0.70	0.67	0.64	0.57
12.0	12.1	12.2	12.3	15.2	15.4	15.4	15.4
1.33	1.27	1.22	1.21	0.78	0.78	0.71	0.65

0.44	0.38	0.31	0.66	0.50	0.45	0.42	0.36
15.6	15.7	15.7	17.5	15.6	17.7	17.7	17.8
0.57	0.57	0.49	0.74	0.62	0.58	0.57	0.53

(Thickness)

Re·10 ⁻³ [-]	0.30	0.26	22.1	20.2	18.1	16.3	
T [°C]	17.8	17.8	15.1	15.1	15.3	15.4	
h [mm]	0.49	0.45	4.91	4.77	4.50	4.32	

14.3	12.4	11.3	10.1	8.74	8.19	7.54	5.74
15.4	15.4	15.5	15.6	15.7	15.7	15.7	15.8
4.01	3.78	3.67	3.43	3.21	2.89	2.22	1.66

4.14	2.58	21.3	20.1	19.0	18.0	16.8	15.8
15.8	15.9	13.9	14.0	14.1	14.3	14.3	14.4
1.47	1.28	5.06	4.80	4.68	4.57	4.43	4.27

14.3	13.1	11.9	11.1	9.63	8.42	7.57	5.38
14.3	14.5	14.5	14.6	14.7	14.7	14.8	14.8
4.07	3.85	3.75	3.59	2.43	3.17	2.31	1.66

3.12	7.88	7.33	6.95	6.65	6.23	5.63	5.22
14.9	11.2	11.4	11.4	11.5	11.6	11.6	11.7
1.34	1.88	1.83	1.75	1.74	1.67	1.62	1.57

(Thickness)

$Re \cdot 10^{-3} [-]$	4.69	4.20	3.68	3.47	0.51	0.45
T [°C]	11.7	11.8	11.8	11.9	16.4	16.5
h [mm]	1.52	1.47	1.43	1.40	0.66	0.63

0.40	0.34	0.30	0.23	0.15	0.62	0.28	0.21
16.6	16.6	16.6	16.6	16.7	14.3	14.8	14.8
0.59	0.57	0.52	0.49	0.44	0.76	0.58	0.51

8.56	7.88	7.14	6.49	6.04	4.97	4.31	3.45
16.9	16.9	17.0	17.0	17.0	17.1	17.1	17.1
1.99	1.85	1.73	1.65	1.62	1.49	1.43	1.33

3.01	2.49	11.4	10.6	10.1	9.45	8.68	8.09
17.1	17.1	14.5	14.6	14.7	14.8	14.9	14.9
1.30	1.24	3.62	3.50	3.45	3.25	2.87	2.51

7.42	6.97
14.9	15.0
2.10	1.99

Positions of Wave Inception x_c

Inclination angle of the plate $\theta=9^\circ$

$Re \cdot 10^{-3} [-]$	0.2	0.3	0.4	0.5	0.6	0.7
x_c [cm]	10	15	15	25	30	30
T [$^\circ$ C]	23.5	24	24	24	24	24

0.8	0.9	1.0	1.5	2.0	2.5	3.0	3.5
35	40	40	60	60	85	100	105
24	24	24	42	25	25	25	25

4.0	4.5	5.0	5.5	6.0	6.5	7.0	7.5
105	115	110	130	130	115	110	110
25.5	25.5	25.5	26	26	26	26	26

8.0	8.5	9.0	9.5	10.0	12.0
105	100	110	115	80	60
26	26	27	27	27	27

$\theta=33^\circ$ (Wave Inception x_c)

$Re \cdot 10^{-3}$ [-]	0.5	0.6	0.7	0.8	0.9	1.0
x_c [cm]	20	20	25	30	30	30
T [$^\circ C$]	27	27	27	27	27	27

1.5	2.0	2.5	3.0	3.5	4.0	4.5	5.0
40	55	60	60	60	60	60	60
27	27	27	27	27	27	27	27

5.5	6.0	6.5	7.0	7.5	8.0	8.5	9.0
60	60	55	60	60	60	60	60
27	25.5	25.5	25.5	24.5	24.5	24.5	24.5

9.5	10.0	12.0
50	50	40
24.5	24.5	23

$\theta=52^\circ$

$Re \cdot 10^{-3}$	1.5	2.0
x_c	50	60
T	18.5	18

2.5	3.0	3.5	4.0	4.5	5.0	5.5	6.0
60	65	60	60	60	60	55	55
18.5	19	20	20	20	20	20	20

($\theta=52^\circ$) (Wave Inception x_c)

6.5	7.0	7.5	8.0	8.5	9.0	9.5	10.0
55	55	60	55	50	50	50	50
20	20	20	20	21	21	21	21

12.0
30
21

Falling Liquid used

$K_4Fe(CN)_6$ $2.0 \cdot 10^{-2}$ mol/l, NaOH 1.0mol/l

$K_3Fe(CN)_6$ $5.9 \cdot 10^{-3}$ mol/l

density 1.06 gr/cm^3 , temperature 25.3°C

viscosity $1.1 \cdot 10^{-2}$ poise

diffusion coefficient $6.8 \cdot 10^{-6} \text{ cm}^2/\text{sec}$

Re=410 (Instantaneous h and k)

t[sec]	0	0.02	0.04	0.06	0.08
$h \cdot 10^{-2}$ [cm]	3.4	3.4	3.0	3.0	3.2
$k \cdot 10^{-4}$ [cm/sec]	8.89	8.89	8.94	8.94	9.04

0.10	0.12	0.14	0.16	0.18	0.20	0.22	0.24
3.2	3.0	3.8	4.1	5.4	5.8	5.4	5.1
9.15	9.26	9.36	9.58	9.47	9.15	8.94	8.94

0.26	0.28	0.30	0.32	0.34	0.36
5.0	4.9	4.9	4.5	4.5	4.5
8.83	8.94	8.94	8.94	8.94	8.94

Re=550

(Instantaneous h and k)

t[sec]	0	0.02	0.04	0.06	0.08
$h \cdot 10^{-2}$ [cm]	4.3	3.8	3.8	3.7	3.4
$k \cdot 10^{-4}$ [cm/sec]	9.26	9.29	9.29	9.36	9.52

0.10	0.12	0.14	0.16	0.18	0.20	0.22	0.24
3.4	5.0	8.5	10.4	9.7	8.2	7.5	6.8
9.55	10.2	10.4	10.2	9.69	9.32	9.23	9.29

0.26	0.28	0.30	0.32	0.34	0.36
5.9	5.2	4.4	3.7	3.7	3.7
9.19	9.19	9.19	9.17	9.17	9.14

Re=610	t	0	0.02	0.04	0.06	0.08
	$h \cdot 10^{-2}$	5.1	5.0	5.0	5.0	5.1
	$k \cdot 10^{-4}$	11.7	11.7	11.9	12.4	12.8

0.10	0.12	0.14	0.16	0.18	0.20	0.22	0.24
7.8	10.4	11.4	11.4	11.0	9.7	8.5	7.8
13.3	13.4	12.7	12.4	12.3	12.2	11.9	11.8

(Instantaneous h and k)

0.26	0.28	0.30
6.7	5.8	5.1
11.7	11.7	11.7

Re=730	t[sec]	0	0.02	0.04
	$h \cdot 10^{-2}$ [cm]	4.1	3.6	3.8
	$k \cdot 10^{-4}$ [cm/sec]	9.2	9.31	9.41

0.06	0.08	0.10	0.12	0.14	0.16	0.18	0.20
3.0	2.8	4.9	8.0	8.3	8.5	8.3	8.0
9.69	10.2	10.7	10.2	10.1	9.70	9.56	9.46

0.22	0.24	0.26	0.28	0.30	0.32	0.34	0.36
7.8	7.2	7.0	6.2	5.8	5.3	4.4	4.2
9.40	9.31	9.21	9.14	9.11	9.14	9.14	9.20

Re=840	0	0.02	0.04	0.06	0.08	0.10
	6.7	5.4	5.1	4.5	3.8	3.8
	11.0	11.0	11.1	11.1	11.1	11.1

(Instantaneous h and k)

0.12	0.14	0.16	0.18	0.20	0.22	0.24	0.26
3.6	3.8	3.6	3.6	10.1	14.6	16.7	17.2
11.3	11.5	12.0	12.8	13.4	12.5	12.3	12.2

0.28	8.30	0.32	0.34	0.36	0.38	0.40	0.42
18.0	19.7	20.6	20.6	18.2	16.3	14.7	12.2
12.3	12.3	11.9	11.8	11.6	11.1	10.8	10.8

0.44	Re=1040	t[sec]	0	0.02
10.4		$h \cdot 10^{-2}$ [cm]	9.7	8.2
11.1		$k \cdot 10^{-4}$ [cm/sec]	10.7	10.7

0.04	0.06	0.08	0.10	0.12	0.14	0.16	0.18
7.5	6.7	6.2	5.4	5.1	4.7	4.7	4.5
11.1	11.2	11.3	11.5	11.5	11.5	11.5	11.8

0.20	0.22	0.24	0.26	0.28	0.30	0.32	0.34
4.5	4.5	14.5	18.5	20.1	20.6	18.9	17.6
12.2	12.4	13.3	12.9	12.5	12.2	11.8	11.6

(Instantaneous h and k)

0.36	0.38	0.40	0.42
16.7	15.0	12.1	10.4
11.7	11.2	10.9	10.8

Re=1250	t[sec]	0	0.02	0.04
	$h \cdot 10^{-2}$ [cm]	12.1	10.8	9.6
	$k \cdot 10^{-4}$ [cm/sec]	9.4	9.7	9.8

0.06	0.08	0.10	0.12	0.14	0.16	0.18	0.20
8.6	7.4	7.6	11.7	17.0	20.3	21.7	21.5
10.3	10.5	11.2	12.6	11.3	10.9	10.4	10.1

0.22	0.24	0.26	0.28	0.30	0.32	0.34	0.36
20.2	18.3	16.6	14.7	12.7	11.2	9.3	8.1
9.6	9.5	9.3	9.3	9.5	9.4	9.4	9.3

0.38	0.40	0.42	0.44
7.4	6.5	5.7	5.2
9.3	9.5	9.7	9.7

PUBLICATION LIST

- (1) Velocity Profile in "Calming Zone" of Falling Liquid Films on Inclined Plates;
Ito, R. and K. Tomura: J. Chem. Eng. Japan, 12, 10~13(1979)
- (2) Thickness of Liquid Falling Films in "Calming Zone" on Inclined Plates;
Ito, R. and K. Tomura: J. Chem. Eng. Japan, 12, 66~68(1979)
- (3) Wave Inception on a Falling Liquid Film;
Ito, R. and K. Tomura: J. Chem. Eng. Japan, (submitted)
- (4) Simultaneous Measurements of Thickness and Local Mass Transfer Rate on Falling Liquid Films;
Ito, R., K. Tomura, M. Yamamoto, N. Tsuboi, T. Nakajima and M. Kawai: J. Chem. Eng. Japan, (submitted)

Acknowledgement

The present work has been carried out under the direction of Professor Ryuzo Ito in his laboratory at Osaka University. It is recorded as a thesis to be submitted to the Faculty of Engineering Science, Osaka University, in fulfillment of requirements for the Degree of Doctor of Engineering at the end of the course of the graduate school.

Professor Ryuzo Ito is thanked for his constant guidance and helpful suggestions throughout this research. Thanks are due to Professor Takashi Katayama, Department of Chemical Engineering, and Professor Tatsuzo Hirose, Professor Tsunehiko Kakutani, Department of Mechanical Engineering, for their helpful suggestions and for reviewing this manuscript.

The author wishes to acknowledge to Mr. Yushi Hirata, Dr. Sadataka Shiba and Mr. Yoshiro Inoue, Assistants at the laboratory, for their advice. Thanks are due to Miss Mari Kamei for her generous assistance in the typing of the manuscript.

The author also wishes to acknowledge to Messrs. Yukie Okada and Yasuyuki Yoshida, for their

experimental assistance.

Finally, author's grateful thanks are also due to his parents, Dr. and Mrs. Teruichi Tomura, and to his brother Satoru for their constant encouragement.